Title

Prosapip1-Dependent Synaptic Adaptations in the Nucleus Accumbens Drive Alcohol Intake, Seeking, and Reward

Journal

Neuron, 96(1)

ISSN

0896-6273

Authors

Laguesse, Sophie
Morisot, Nadege
Shin, Jung Hoon
et al.

Publication Date

2017-09-01

DOI

10.1016/j.neuron.2017.08.037

Peer reviewed

Article

Neuron

Prosapip1-Dependent Synaptic Adaptations in the Nucleus Accumbens Drive Alcohol Intake, Seeking, and Reward

Highlights

- Alcohol intake initiates mTORC1-dependent translation of Prosapip1 in the NAc
- Prosapip1 contributes to alcohol-dependent actin dynamics and spine morphology
- Alcohol-dependent synaptic localization of GluA2-lacking AMPAR requires Prosapip1
- Prosapip1-dependent cellular adaptations drive alcohol seeking, drinking, and reward

Authors

Sophie Laguesse, Nadege Morisot, Jung Hoon Shin, ..., Kevin J. Bender, Veronica A. Alvarez, Dorit Ron

Correspondence

dorit.ron@ucsf.edu

In Brief

Laguesse et al. identified Prosapip1 as a novel downstream target of mTORC1 in the nucleus accumbens that promotes actin reorganization as well as morphological and synaptic alterations that in turn drive alcohol drinking and seeking behaviors.

Laguesse et al., 2017, Neuron *96*, 145–159
September 27, 2017
http://dx.doi.org/10.1016/j.neuron.2017.08.037

CellPress

Neuron
Article

Prosapip1-Dependent Synaptic Adaptations in the Nucleus Accumbens Drive Alcohol Intake, Seeking, and Reward

Sophie Laguesse,[1] Nadege Morisot,[1,6,7] Jung Hoon Shin,[2,6] Feng Liu,[1,8] Martin F. Adrover,[2] Samuel A. Sakhai,[1] Marcelo F. Lopez,[3] Khanhky Phamluong,[1] William C. Griffin III,[3] Howard C. Becker,[3,4,5] Kevin J. Bender,[1] Veronica A. Alvarez,[2] and Dorit Ron[1,9,*]

[1]Department of Neurology, University of California, San Francisco, CA, USA
[2]Laboratory on Neurobiology of Compulsive Behaviors, National Institute of Alcohol Abuse and Alcoholism, US National Institutes of Health, Bethesda, MD, USA
[3]Charleston Alcohol Research Center, Department of Psychiatry and Behavioral Sciences, Medical University of South Carolina, Charleston, SC, USA
[4]Department of Neurosciences, Medical University of South Carolina, Charleston, SC, USA
[5]RHJ Department of Veterans Affairs Medical Center, Charleston, SC, USA
[6]These authors contributed equally
[7]Present address: N.M. Brains On-line LLC, South San Francisco, CA, United States
[8]Present address: School of Life Sciences, Sun Yat-sen University, Guangzhou, China
[9]Lead Contact
*Correspondence: dorit.ron@ucsf.edu
http://dx.doi.org/10.1016/j.neuron.2017.08.037

SUMMARY

The mammalian target of rapamycin complex 1 (mTORC1), a transducer of local dendritic translation, participates in learning and memory processes as well as in mechanisms underlying alcohol-drinking behaviors. Using an unbiased RNA-seq approach, we identified Prosapip1 as a novel downstream target of mTORC1 whose translation and consequent synaptic protein expression are increased in the nucleus accumbens (NAc) of mice excessively consuming alcohol. We demonstrate that alcohol-dependent increases in Prosapip1 levels promote the formation of actin filaments, leading to changes in dendritic spine morphology of NAc medium spiny neurons (MSNs). We further demonstrate that Prosapip1 is required for alcohol-dependent synaptic localization of GluA2 lacking AMPA receptors in NAc shell MSNs. Finally, we present data implicating Prosapip1 in mechanisms underlying alcohol self-administration and reward. Together, these data suggest that Prosapip1 in the NAc is a molecular transducer of structural and synaptic alterations that drive and/or maintain excessive alcohol use.

INTRODUCTION

Drugs of abuse are thought to usurp normal learning and memory in brain circuits involved in motivation, reinforcement, and decision making (Hyman, 2005). Long-lasting synaptic changes are required for learning and memory processes, which in part depend on the local translation of proteins at dendrites (Buffington et al., 2014). A major contributor to the local translation of synaptic proteins is the mammalian target of rapamycin (mTOR) complex 1 (mTORC1) (Buffington et al., 2014). mTOR is a serine and threonine kinase that associates with the regulatory associated protein of TOR (Raptor), as well as other adaptor proteins and enzymes to form the mTORC1 complex (Ma and Blenis, 2009). Activation of signaling pathways, predominantly the Phosphoinositide 3-kinase (PI3K)/AKT pathway, activates mTORC1 (Ma and Blenis, 2009). mTORC1 phosphorylates the p70 ribosomal S6 kinase (S6K) and the eukaryotic translation initiation factor 4E binding protein (4E-BP), and these phosphorylation events promote the assembly of the translation initiation complex to initiate cap-dependent mRNA translation (Sonenberg and Hinnebusch, 2009). mTORC1 has been shown to be a focal point in mechanisms underlying the actions of drugs of abuse (Neasta et al., 2014). However, how mTORC1 signaling regulates synaptic functions, especially in the context of addiction, is not entirely clear. Furthermore, knowledge regarding the translation profile of mTORC1 in the central nervous system (CNS) is limited.

We previously found that excessive alcohol consumption activates the PI3K/AKT pathway in the nucleus accumbens (NAc) of rodents resulting in the activation of mTORC1 (Beckley et al., 2016; Laguesse et al., 2016; Liu et al., 2017; Neasta et al., 2010). We further demonstrated that intra-NAc or systemic administration of the selective mTORC1 inhibitors attenuates alcohol seeking and drinking (Beckley et al., 2016; Neasta et al., 2010; Morisot et al., 2017). Finally, we identified a role for mTORC1 in the reconsolidation of alcohol seeking memories (Barak et al., 2013). Together, these data suggest that mTORC1 plays a central role in neuroadaptations underlying alcohol-drinking behaviors.

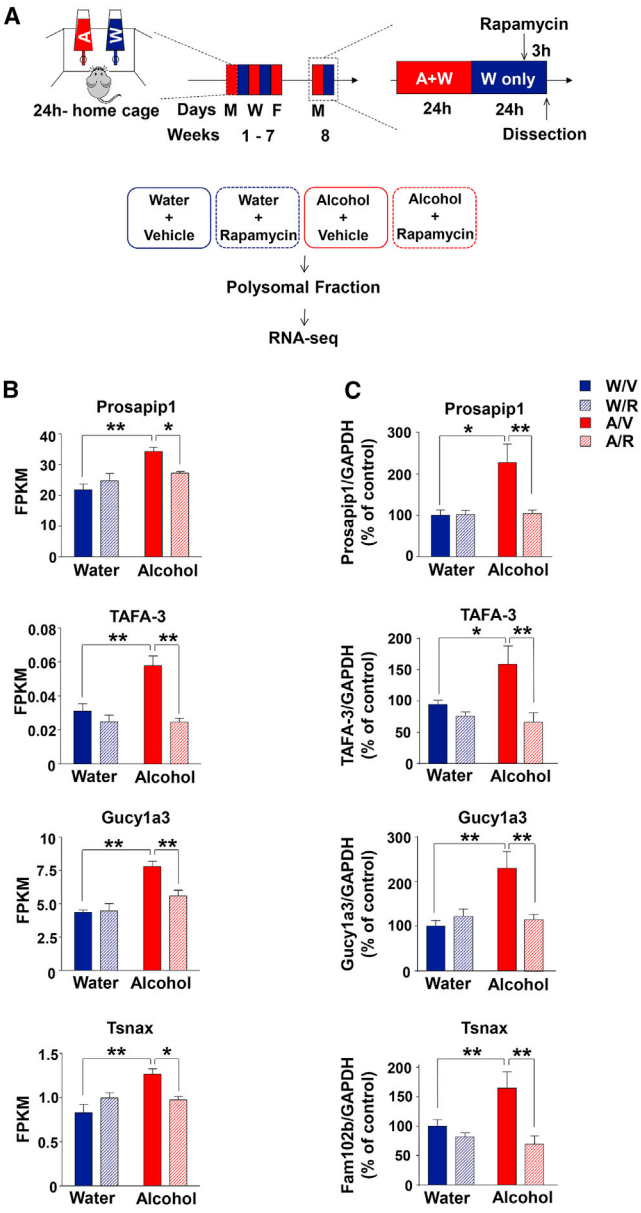

Figure 1. RNA-Seq Identified mRNAs Whose Translation Is Increased by Alcohol and depends on mTORC1 Activity in the NAc

(A) Mice experienced 7–8 weeks of IA20%-2BC. Control animals had access to water only. Three hours before the end of the last 24 hr of alcohol withdrawal, mice were systemically administered with 20 mg/kg of rapamycin or vehicle. The NAc from the four groups of mice (water/vehicle [blue], water/rapamycin [hatched blue], alcohol/vehicle [red], alcohol/rapamycin [hatched red]) were dissected 3 hr after the administration of rapamycin and were subjected to polysomal purification and RNA-seq analysis.

(B) RNA-seq data depicting fragments per kilobase of transcript per million mapped reads (FPKM) value of *Prosapip1*, *TAFA-3*, *Gucy1a3*, and *Tsnax*. Data are presented as the average FPKM value ± SEM and expressed as the percentage of water/vehicle. Two-way ANOVA showed a significant interaction between alcohol and rapamycin (respectively, *Prosapip1* $F_{(1,8)}$ = 8.874, p = 0.018; *TAFA-3* $F_{(1,8)}$ = 10.02, p = 0.013, *Gucy1a3* $F_{(1,8)}$ = 7.98, p = 0.022; *Tsnax* $F_{(1,8)}$ = 11.83, p = 0.009) and post hoc Student–Newman–Keuls test detected a significant difference between water and alcohol within the vehicle group (respectively, *Prosapip1* *p* = 0.003; *TAFA-3* p = 0.002; *Gucy1a3* p = 0.002; *Tsnax* p = 0.007) and a significant difference between vehicle and rapamycin within the alcohol group (respectively, *Prosapip1* p = 0.018; *TAFA-3* p = 0.003; *Gucy1a3* p = 0.005; *Tsnax* p = 0.04). n = 3.

(C) A new cohort of animals that underwent the same paradigm described in (A) was used to measure polysomal mRNA level of *Prosapip1*, *TAFA-3*, *Gucy1a3*, and *Tsnax* by qRT-PCR. Data are presented as the average ratio of each transcript to *GAPDH* ± SEM, and expressed as the percentage of water/vehicle. Two-way ANOVA showed a significant interaction between alcohol and rapamycin (respectively, *Prosapip1* $F_{(1,16)}$ = 5.943, p = 0.027; *TAFA-3* $F_{(1,16)}$ = 4.654, p = 0.047, *Gucy1a3* $F_{(1,28)}$ = 7.6, p = 0.01; *Tsnax* $F_{(1,28)}$ = 6.97, p = 0.013) and post hoc Student–Newman–Keuls test detected a significant difference between water and alcohol within the vehicle group (respectively, *Prosapip1* p = 0.013; *TAFA-3* p = 0.017; *Gucy1a3* *p* = 0.006; *Tsnax* p = 0.005) and a significant difference between vehicle and rapamycin within the alcohol group (respectively, *Prosapip1* p = 0.004; *TAFA-3* p = 0.007; *Gucy1a3* p = 0.007; *Tsnax* p = 0.007). n = 5 for *Prosapip1* and *TAFA-3*; n = 8 for *Gucy1a3* and *Tsnax*. *p < 0.05, **p < 0.01.

Here, we set to identify downstream transducers of mTORC1 in the NAc that drive and maintain alcohol-dependent behavioral phenotypes. To do so, we isolated polysomes, which contain mRNAs actively undergoing translation (del Prete et al., 2007), from the NAc of mice that have been consuming large amounts of alcohol for 8 weeks and utilized a high-throughput RNA sequencing (RNA-seq) approach to identify mRNAs whose translation is increased by alcohol in an mTORC1-dependent manner. Among the identified candidates was *Prosap2-interacting protein 1* (*Prosapip1*).

Prosapip1 is a brain-specific protein that is highly enriched in the postsynaptic density (PSD) of hippocampal neurons (Wendholt et al., 2006). Prosapip1 belongs to the Fezzin family of proteins, all of which contain a Fez domain and a coiled-coil domain enabling the formation of homo- and heterodimers (Reim et al., 2016; Wendholt et al., 2006). First identified as a binding partner for Shank3 (Prosap2) in hippocampal neurons (Wendholt et al., 2006), Prosapip1 has also been shown to interact with the spine-associated Rap GTPase-activating protein (SPAR). Prosapip1 association with SPAR regulates SPAR's post-synaptic localization (Reim et al., 2016; Wendholt et al., 2006). Here, we report that Prosapip1 contributes to synaptic and structural modification in NAc neurons and, by doing so, the protein plays an important role in alcohol reward-seeking behaviors.

RESULTS

Identification of mTORC1-Dependent Candidate Transcripts Whose Translation Is Increased by Alcohol

To identify novel mTORC1-dependent mRNAs whose translation is induced in response to heavy alcohol use, mice underwent an intermittent access to 20% alcohol in a 2-bottle choice (IA20%-2BC) paradigm for 8 weeks during which animals consumed large quantities of alcohol (17.08 ± 0.53 g/kg/24 hr). Control animals had free access to water only. Three hours before the end of the last 24-hr alcohol withdrawal session, mice were systemically administered with vehicle or the specific inhibitor of mTORC1, rapamycin (Li et al., 2014). The NAc was removed 24 hr after the end of the last drinking session, polysomes were purified, and Illumina high-throughput RNA-seq was performed (Figure 1A).

Table 1. Transcripts Showing mTORC1-Dependent Increased Translation after Excessive Alcohol Drinking Identified by RNA-Seq

Gene ID	Gene Accession Number	Gene Name	Folds Alcohol	p Value Alcohol	Folds Rapamycin	p Value Rapamycin
Tnrc6a	GenBank: NM_144925	trinucleotide repeat containing 6a	10.98	0.006	−10.35	0.004
Cnot4	GenBank: NM_001164412	CCR4-NOT transcription complex, subunit 4 (Not4)	3.29	0.030	−3.50	0.019
Inpp5b	GenBank: NM_008385	inositol polyphosphate-5-phosphatase B	2.99	0.042	−3.03	0.016
Ndufs1	GenBank: NM_001160038	NADH dehydrogenase Fe-S protein 1	2.96	0.010	−2.71	0.038
RasGrp4	GenBank: NR_045676	Ras guanyl releasing protein 4	2.80	0.032	−1.93	0.006
Cyp2a5	GenBank: NM_007812	cytochrome P450, family 2a, polypeptide 5	2.76	0.024	−1.95	0.017
Pdk3	GenBank: NM_145630	pyruvate dehydrogenase kinase, isoenzyme 3	2.01	0.015	−1.82	0.042
TAFA3	GenBank: NM_183224	family with sequence similarity 19, member A3	1.87	0.019	−2.35	0.005
Gucy1a3	GenBank: NM_021896	guanylate cyclase 1, soluble, alpha 3	1.79	0.001	−1.39	0.019
Prosapip1	GenBank: NM_197945	proSAP (Shank3)-interacting protein 1	1.57	0.005	−1.26	0.010
Fam102b	GenBank: NM_001163567	family with sequence similarity 102, member B	1.56	0.006	−1.27	0.049
Tsnax	GenBank: NM_016909	translin-associated factor X	1.53	0.017	−1.30	0.016

Data are sorted in ascending order of fold change (alcohol/vehicle divided by water/vehicle) with positive values indicating an increased translation by alcohol. Fold change (alcohol/vehicle divided by alcohol/rapamycin) with negative values indicate a decreased translation by rapamycin. Two-way ANOVA and Student-Newman-Keuls test (n = 3). NADH, nicotinamide adenine dinucleotide; ATP, adenosine triphosphate; cGMP, cyclic guanosine monophosphate.

RNA-seq analysis revealed 421 transcripts whose translation was increased by alcohol by at least 1.5-fold in the "Alcohol/Vehicle" group compared to the "Water/Vehicle" group. Among those, 12 transcripts exhibited a >1.25-fold decrease in translation in the "Alcohol/Rapamycin" group compared to "Alcohol/Vehicle" group (Table 1). RNA-seq data of four transcripts (Figure 1B) were then confirmed by quantitative real-time PCR (qRT-PCR) (Figure 1C). Specifically, alcohol increased the polysomal mRNA content of the brain-specific secretory peptide TAFA-3 (Fischer et al., 2012; Tom Tang et al., 2004), the guanylate cyclase 1 soluble subunit alpha (Gucy1a3), which catalyzes the generation of the second messenger cGMP from GTP (Potter, 2011), the translin-associated factor x (Tsnax) that mediates RNA trafficking in neurons (Li et al., 2008), and the scaffolding protein Prosapip1 (Reim et al., 2016; Wendholt et al., 2006) (Figures 1B and 1C). Alcohol-mediated increase in the translation of the mRNAs was inhibited by rapamycin and thus was dependent on mTORC1 activation (Figures 1B and 1C).

Excessive Alcohol Intake Increases the Translation of Prosapip1 in the NAc

We chose to follow upon the candidate transcript, *Prosapip1*, which we found to be highly expressed in the striatum (Figure S1A). To determine whether the increases in *Prosapip1* in the polysomal fraction were due solely to increased translation, we compared the level of the *Prosapip1* mRNA in the polysomal fraction versus the total mRNA levels. We found that binge drinking of alcohol increased *Prosapip1* levels only in the polysomal fraction, whereas the total mRNA quantity was unaltered (Figures 2A and 2B). Rapamycin did not alter the total mRNA levels of *Prosapip1* in the presence or absence of alcohol (Figure S1B), indicating that alcohol induced an increase in *Prosapip1* translation without a change at the transcriptional level. In addition, rapamycin, even at a high dose (40 mk/kg), did not alter the translation of *Prosapip1* in water-only-consuming animals (Figure S1C), suggesting that long-term alcohol intake that activates mTORC1 in the NAc (Laguesse et al., 2016; Neasta et al., 2010) is a prerequisite for mTORC1-dependent translation of Prosapip1.

Next, we tested whether the increase in the polysomal mRNA of *Prosapip1* corresponds with an increase in the level of the protein. As Prosapip1 is enriched in the PSD (Wendholt et al., 2006), we analyzed its protein levels in both the total homogenate and in the crude synaptosomal fraction. As shown in Figures 2C and 2D, binge drinking of alcohol increased the protein levels of Prosapip1 in both the total homogenate and the synaptosomal fraction, an increase that was maintained even after 24 hr of withdrawal (Figures 2E and 2F). Prosapip1 levels were not elevated in response to the consumption of moderate amounts of alcohol (Figure S2A), suggesting that alcohol exposure per se does not affect Prosapip1 expression, but rather the high level of intake, accompanied by cycles of binge and withdrawal periods. We further measured Prosapip1 levels in the NAc of mice consuming other rewarding solutions saccharin and sucrose and observed no change in the level of the protein as compared to water only drinking mice (Figures S2B and S2C), suggesting that the alcohol-dependent increase in Prosapip1 translation is not a common mechanism shared by other rewarding substances. To test for brain region specificity, we measured the level of the protein in the two other striatal regions, the dorsomedial striatum (DMS) and the dorsolateral striatum (DLS). In line with the observation that alcohol does not activate mTORC1 in the DMS and DLS (Laguesse et al., 2016), Prosapip1 levels were unaltered by alcohol in either striatal regions (Figures S2D and S2E). Together, these data suggest that the translation of Prosapip1 is selectively induced in the NAc in response to chronic intermittent consumption of high levels of alcohol.

Prosapip1 Contributes to Actin Dynamics

In hippocampal neurons, Prosapip1 interacts with members of the spine-associated RapGAP (SPAR) proteins, which also reside in the PSD (Reim et al., 2016; Wendholt et al.,

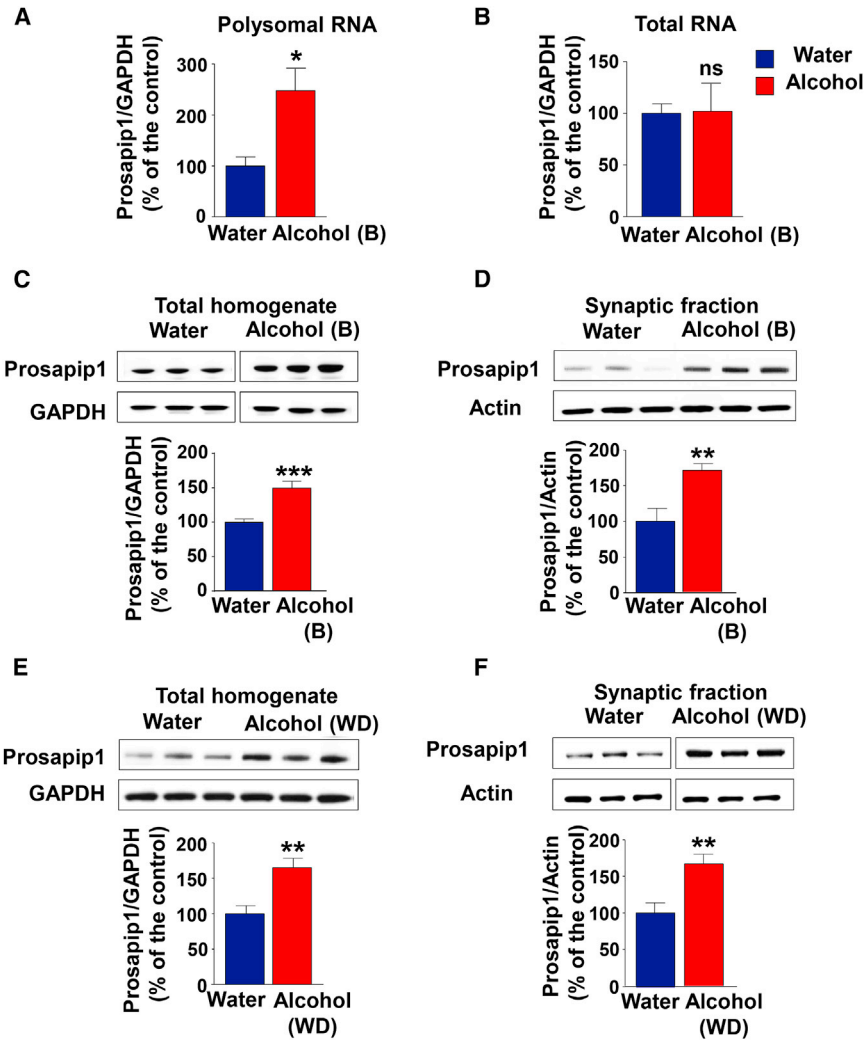

Figure 2. Alcohol-Dependent Translation of Prosapip1 Corresponds to Increases in Protein Levels that Are Maintained during Withdrawal

After 7–8 weeks of IA20%-2BC, NAc of mice were dissected 4 hr after the beginning (Binge, B) (A–D) or 24 hr after the end of the last drinking session (Withdrawal, WD) (E and F). Control animals had access to water only.

(A and B) *Prosapip1* mRNA levels in response to a binge session were determined by qRT-PCR in the polysomal fraction (A) and total fraction (B). Data are presented as the average ratio of *Prosapip1* to *GAPDH* ± SEM and expressed as the percentage of water control. Significance was determined using two-tailed unpaired t test. (A) polysomal *Prosapip1* mRNA $t_{(6)}$ = 3.207, p = 0.0184. n = 4. (B) total *Prosapip1* mRNA $t_{(6)}$ = 0.07, p = 0.9464. n = 4.

(C–F) Prosapip1 protein levels after binge (C and D) and withdrawal (E and F) were determined by western blot analysis. ImageJ was used for optical density quantification. Data are presented as the average ratio of Prosapip1 to GAPDH ± SEM (C and E) or Prosapip1 to actin ± SEM (D and F) and are expressed as the percentage of water control. Significance was determined using two-tailed unpaired t test. Prosapip1 in the total homogenate (C) $t_{(14)}$ = 4.359, p = 0.0007, n = 8 per group; and in the synaptic fraction (D) $t_{(7)}$ = 3.7, p = 0.0077, n = 4 water, 5 binge. Prosapip1 in the total homogenate (E) $t_{(15)}$ = 3.656, p = 0.0023, n = 8 water, 9 withdrawal; and in the synaptic fraction (F) $t_{(7)}$ = 3.515, p = 0.0098. n = 4 water, 5 withdrawal. *p < 0.05, **p < 0.01, ***p < 0.001.

2006). We first confirmed that Prosapip1 associates with SPAR in Neuroblastoma 2A (N2A) cells (Figures S3A–S3D), and found that the association of Prosapip1 and SPAR is also detected in the NAc (Figures S3E and S3F). SPAR is a GTPase-activating protein (GAP) for Rap, a small G protein that participates in the reorganization of actin (Spilker and Kreutz, 2010). We therefore hypothesized that Prosapip1 may play a role in actin dynamics. To test this possibility, we transfected N2A cells with a plasmid expressing Prosapip1 or a plasmid expressing a short hairpin RNA (shRNA) sequence targeting the Prosapip1 transcript (shProsapip1), and measured the amount of Globular actin (G-actin) versus Filamentous actin (F-actin) following gene manipulation. We found that overexpression of Prosapip1 increased (Figure 3A), whereas downregulation of the protein decreased (Figure 3B) F-actin content. These data suggest that Prosapip1 promotes F-actin assembly. Next, to test the consequences of Prosapip1 manipulation on actin dynamics *in vivo*, the NAc of mice was infected with a lentivirus (Ltv) expressing Prosapip1 (Ltv-Prosapip1) or a control virus expressing GFP only (Ltv-CTL), and a lentivirus expressing shProsapip1 (Ltv-shProsapip1) or a scrambled sequence control (Ltv-SCR) (Figure S4), and the relative amounts of F- and G-actin were measured. We found that overexpression of Prosapip1 in the NAc significantly increased F-actin content at the expense of G-actin (Figure 3C), whereas Prosapip1 knockdown led to a decrease in F-actin and an increase in G-actin content (Figure 3D). Together, these data suggest that Prosapip1 in the NAc plays a prominent role in actin dynamics.

Alcohol Consumption Increases F-actin Content via Prosapip1

Next, we postulated that alcohol alters F-actin dynamics via Prosapip1. We therefore analyzed the F/G actin ratio in the NAc of mice after binge drinking of alcohol. As shown in Figure 3E, alcohol significantly increased F-actin content in the NAc of mice consuming alcohol compared to water controls. In order to determine whether excessive alcohol drinking increases F-actin content via Prosapip1, we measured F- and G-actin ratio in the NAc of mice exposed to alcohol and infected with Ltv-shProsapip1 or Ltv-SCR. To avoid any bias that could result from a reduced amount of alcohol voluntary consumed by mice infected with Ltv-shProsapip1, mice underwent 2 weeks

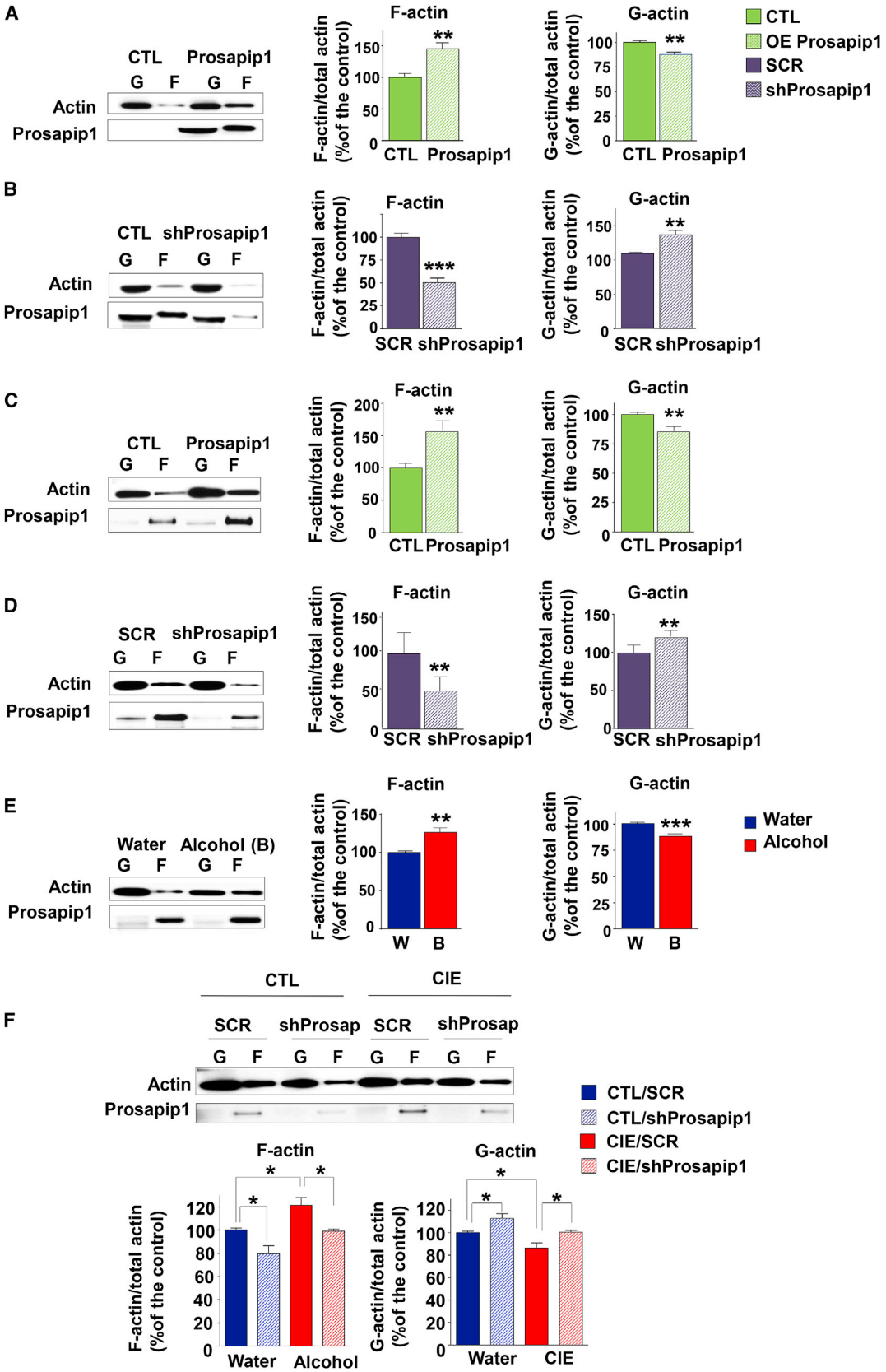

(legend on next page)

of non-contingent chronic intermittent exposure (CIE) to alcohol vapor (Becker and Lopez, 2004) (Figure S5A). First, we confirmed that 2 weeks of CIE exposure to alcohol activates mTORC1 and increase Prosapip1 levels in the NAc as compared to control mice (Figure S5B). We then analyzed the G-actin and F-actin content after CIE exposure in mice infected with Ltv-shProsapip1 or Ltv-SCR. As shown in Figure 3F, we found that shProsapip1 counteracted the increase in F-actin content induced by alcohol, with F- and G-actin levels similar to the air exposed controls. Together, these data suggest that Prosapip1 is required for the formation of actin filaments and that alcohol consumption increases F-actin content in the NAc via Prosapip1.

Alcohol-Dependent Alterations of Dendritic Spine Morphology depend on Prosapip1

Dendritic spines contain a highly dense mesh of actin filaments (Hotulainen and Hoogenraad, 2010). The head and the tip of the spine contain branched actin filaments, whereas the spine neck contains long loosely arranged filaments (Hotulainen and Hoogenraad, 2010). Spine enlargement depends on F-actin assembly and stabilization, while spine shrinkage and elimination require F-actin disassembly (Cingolani and Goda, 2008). Given that Prosapip1 plays a role in F-actin assembly and that excessive alcohol drinking promotes the formation of actin filaments via Prosapip1, we hypothesized that the consequences of alcohol-dependent alterations in actin dynamics are morphological modifications at dendrites, which depend on Prosapip1. Following 4 weeks of IA20%-2BC paradigm, the NAc of alcohol- or water-consuming mice was infected bilaterally with a low titer (1×10^5 pg/mL) of Ltv-shProsapip1 or Ltv-SCR. Following 1 week of recovery, IA20%-2BC was resumed for 3 weeks (Figure 4A). The low viral titer was used in order to avoid bias resulting from potential reduction in alcohol intake in response to Prosapip1 knockdown in the NAc. Infusion of Ltv-shProsapip1 at a low titer did not affect alcohol intake as measured 3 weeks following surgery (Ltv-SCR: 15.1 ± 1.57 g/kg/24 hr; Ltv-shProsapip1: 14.5 ± 0.97 g/kg/24 hr; $t_{(7)} = 0.26$, $p = 0.80$). Low titer infection also allowed the labeling of a low number of neurons, ensuring the imaging and analysis of dendritic segments bearing spines (Figure S6A). Sholl analysis revealed no change in the length (Figure S6B) or complexity (Figures S6C–S6E) of the dendritic branches among the four conditions.

We then analyzed dendritic spines characteristics. Figure 4B shows representative images of a third-order dendritic branch of infected neurons bearing dendritic spines of the four conditions (Water/Ltv-SCR, Water/Ltv-shProsapip1, Alcohol/Ltv-SCR, Alcohol/Ltv-shProsapip1). Spine density (Figure S6F) and spine length (Figure S6G) were not significantly different between the four groups. However, knockdown of Prosapip1 significantly reduced the spine area (Figure 4C, Water, Ltv-SCR versus Ltv-shProsapip1), suggesting that as predicted, Propapip1 in the NAc plays a role in dendritic spine morphology. Alcohol intake significantly increased the spine area (Figure 4C, Water Ltv-SCR versus Alcohol Ltv-SCR), and importantly, knockdown of Prosapip1 in the presence of alcohol rescued the alcohol-dependent phenotype (Figure 4C, Alcohol Ltv-SCR versus Alcohol Ltv-shProsapip1). These changes observed in spine area were not the result of different levels of GFP in dendritic spines, as GFP intensities in the parent dendritic branch were identical across groups (Figure S6H).

Dendritic spines can be classified into four subclasses: filopodia-, thin-, stubby-, and mushroom-type spines (Kasai et al., 2003). We found that downregulation of Prosapip1 in the NAc increased the number of thin- and filopodia-type spines and decreased the number of mushroom spines (Figure 4D, Water, Ltv-SCR versus Ltv-shProsapip1). Alcohol consumption resulted in an opposite pattern: increased proportion of mushroom-type spines at the expense of thin spines (Figure 4D, Water Ltv-SCR versus Alcohol Ltv-SCR). Importantly, the alcohol-mediated changes in spine structure were not observed in the NAc of mice infected with Ltv-shProsapip1 (Figure 4C, Alcohol Ltv-SCR versus Alcohol Ltv-shProsapip1). Together, these results suggest that the consequence of Prosapip-1-mediated increase in F-actin content is the formation and/or stabilization mushroom-type spines. Our results further suggest that alcohol produces similar modifications of dendritic spine structure toward an enlargement of spines, a phenotype that is mediated by Prosapip1.

Figure 3. Prosapip1 Affects Actin Dynamics and Alcohol Drinking Promotes F-actin Assembly via Prosapip1

(A and B) F- and G-actin content in N2A cells after Prosapip1 transfection without (A, hatched green) and with (B, hatched purple) co-transfection with a shRNA sequence targeting Prosapip1 (shProsapip1), compared to cell expressing the empty plasmid (CTL) (A, green) or a scrambled sequence (SCR, purple) (B). F- and G-actin contents were determined by western blot analysis, and quantification was conducted as in Figure 2. Data are presented as the average ratio of F-actin or G-actin to total actin (F+G) ± SEM and expressed as the percentage of the corresponding control. Significance was determined using two-tailed unpaired t test. (A) F-actin $t_{(10)} = 4.255$, $p = 0.0017$; G-actin $t_{(10)} = 40.255$, $p = 0.0017$. n = 6. (B) F-actin $t_{(6)} = 7.714$, $p = 0.0002$; G-actin $t_{(6)} = 4.22$, $p = 0.0056$. n = 4.

(C and D) F- and G-actin content after bilateral infection of NAc neurons with a lentivirus expressing Prosapip1 (Prosapip1, hatched green) or an empty GFP plasmid (CTL, green) (1×10^8 pg/mL) (C), or after infection with Ltv-shProsapip1 (shProsapip1, hatched purple) or Ltv-SCR (SCR, purple) (1×10^8 pg/mL).

(E) F- and G-actin contents were determined in the NAc of mice after binge drinking of alcohol and in the water control group. Data are presented as the average ratio of F-actin or G-actin to total actin (F + G) ± SEM and expressed as the percentage of the corresponding control. Significance was determined using two-tailed unpaired t test. (C) F-actin $t_{(7)} = 3.52$, $p = 0.0097$; G-actin $t_{(7)} = 3.52$, $p = 0.0097$, n = 4 Ltv-Prosapip1, 5 Ltv-CTL. (D) F-actin $t_{(8)} = 3.389$, $p = 0.0095$; G-actin $t_{(8)} = 3.389$, $p = 0.0095$, n = 5 per group. (E) F-actin $t_{(10)} = 4.078$, $p = 0.0022$; G-actin $t_{(10)} = 5.098$, $p = 0.0005$, n = 6 per group.

(F) The NAc of mice were infused with Ltv-SCR or Ltv-shProsapip1 (1×10^8 pg/mL). Three weeks after surgery, mice underwent 2 weeks of CIE exposure or air exposure as control (CTL) (Figure S5A) and F- and G-actin content were determined as described above. Two-way ANOVA showed a significant main effect of CIE (F-actin: $F_{(1,12)} = 16.83$, $p < 0.01$) and shProsapip1 (F-actin: $F_{(1,12)} = 18.18$, $p < 0.01$;) but no significant interaction (F-actin: $F_{(1,12)} = 0.04$, $p = 0.85$). *Post hoc* Student-Newman-Keuls test detected a significant difference between air and CIE within the SCR group (CTL/SCR versus CIE/SCR, $p < 0.05$), a significant difference between SCR and shProsapip1 within the air group (CTL/SCR versus CTL/shProsapip1, $p < 0.05$) and within the CIE group (CIE/SCR versus CIE/shProsapip1, $p < 0.05$). *$p < 0.05$, **$p < 0.01$, ***$p < 0.001$.

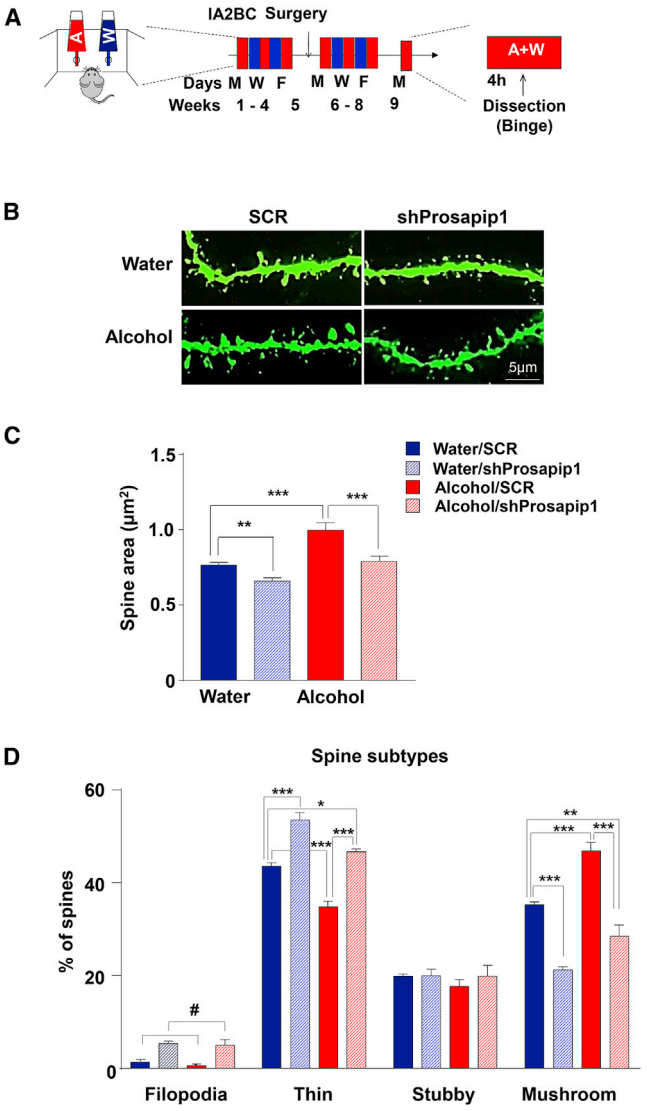

Figure 4. Prosapip1 in the NAc Contributes to Dendritic Spine Morphology and Alterations of Spine Structure by Alcohol Are Mediated by Prosapip1

(A) Mice underwent 4 weeks of IA20%-2BC. Mice consuming water only were used as control. Ltv-shProsapip1 or Ltv-SCR at low titer (1×10^5 pg/mL) was infused into the NAc and after 1 week of recovery, mice were subjected to 3 more weeks of IA20%-2BC. Infection of the NAc with a low titer of Ltv-shProsapip1 did not affect alcohol intake (Ltv-SCR: 15.1 ± 1.57 g/kg/24 hr, Ltv-shProsapip1: 14.5 ± 0.97 g/kg/24 hr). Four hours after the beginning of the last drinking session, mice were transcardially perfused, and MSN morphology was analyzed in NAc shell.

(B) Representative ×100 confocal z stack images of dendritic segments bearing spines for all four experimental conditions. Scale bar, 5 μm.

(C) Average spine area of NAc shell MSNs of mice (Water/SCR [blue], Water/shProsapip1 [hatched blue], Alcohol/SCR [red], Alcohol/shProsapip1 [hatched red]). Data are presented as average spine area ± SEM and are expressed in μm^2. Two-way ANOVA showed a significant main effect of alcohol ($F_{(1,23)}$ = 33.16, $p < 0.001$) and shProsapip1 ($F_{(1,23)} = 31.19$, $p < 0.001$) but no interaction ($F_{(1,23)}$ = 1.052, p = 0.32). *Post hoc* Student-Newman-Keuls test detected a significant difference between water and alcohol in the SCR group (Water/SCR versus Alcohol/SCR, $p < 0.001$), a significant difference between SCR and shProsapip1 within the water group (Water/SCR versus Water/shProsapip1, $p < 0.01$), and within the alcohol group (Alcohol/SCR versus Alcohol/shProsapip1, $p < 0.001$), but no difference between Water/SCR and Alcohol/shProsapip1 (p = 0.903).

(D) Percentage of filopodia, thin, stubby, and mushroom-type spines of NAc shell MSNs. Data are presented as the average percentage of each type of spines across the four conditions ± SEM. Filopodia-type spines, two-way ANOVA showed a significant main effect of shProsapip1 ($F_{(1,23)}$ = 30.14, $p < 0.001$) but no main effect of alcohol ($F_{(1,23)} = 0.67$, p = 0.42) and no interaction ($F_{(1,23)} = 0.09$, p = 0.76); thin spines, two-way ANOVA showed a significant main effect of alcohol ($F_{(1,23)}$ = 47.66, $p < 0.001$) and shProsapip1 ($F_{(1,23)} = 104.6$, $p < 0.001$) but no interaction ($F_{(1,23)} = 0.32$, p = 0.58). *Post hoc* Student-Newman-Keuls test detected a significant difference between water and alcohol within the SCR group (Water/SCR versus Alcohol/SCR, $p < 0.001$), between SCR and shProsapip1 within the water group (Water/SCR versus Water/shProsapip1, $p < 0.001$) and within the alcohol group (Alcohol/SCR versus Alcohol/shProsapip1, $p < 0.001$), and a significant difference between Water/SCR and Alcohol/shProsapip1 ($p < 0.05$); stubby spines, two-way ANOVA showed no significant main effect of alcohol ($F_{(1,23)} = 0.38$, p = 0.55) or shProsapip1 ($F_{(1,23)} = 0.63$, p = 0.43) and no interaction ($F_{(1,23)} = 0.30$, p = 0.58); mushroom spines, two-way ANOVA showed a significant main effect of alcohol ($F_{(1,23)} = 36.71$, $p < 0.001$) and shProsapip1 ($F_{(1,23)} = 103$, $p < 0.001$) but no interaction ($F_{(1,23)} = 2.15$, p = 0.15). *Post hoc* Student-Newman-Keuls test detected a significant difference between water and alcohol within the SCR group (Water/SCR versus Alcohol/SCR, $p < 0.001$), between SCR and shProsapip1 within the water group (Water/SCR versus Water/shProsapip1, $p < 0.001$) and within the alcohol group (Alcohol/SCR versus Alcohol/shProsapip1, $p < 0.001$), and a significant difference between Water/SCR and Alcohol/shProsapip1 ($p < 0.01$). n = 6–9 neurons, n = 4 mice per group. *$p < 0.05$, **$p < 0.01$, ***$p < 0.001$.

Prosapip1 in the NAc Shell Contributes to Alcohol-Dependent Changes in AMPA Receptor Subunit Composition

The actin cytoskeleton plays an important role in AMPA receptor (AMPAR) mobilization and trafficking (Hanley, 2014). We therefore postulated that as Prosapip1 participates in actin dynamics, it may also play a role in the synaptic membranal localization of AMPARs. To test this possibility, we determined the consequences of Prosapip1 knockdown in the NAc on AMPAR synaptic transmission. First, Ltv-SCR and Ltv-shProsapip1 were infused in the NAc shell of water drinking mice. Three weeks after the infusion, whole-cell voltage-clamp recordings were obtained from fluorescently positive MSNs in the NAc shell, and glutamate receptor-mediated synaptic responses were isolated in the presence of the $GABA_A$-receptor blocker gabazine. Excitatory postsynaptic currents (EPSCs) were evoked by electrical stimulation and the ratio of the AMPAR to the NMDA-receptor (NMDAR)-mediated EPSCs, and the rectification properties of the AMPAR synaptic currents were measured. There was no significant change in the mean AMPA/NMDA ratio between the mice infected with Ltv-shProsapip1 in the NAc and mice infected with Ltv-SCR (Figures S7A and S7B). Interestingly, knockdown of Prosapip1 resulted in significant reduction in the rectification index (Figures 5A and 5B). Specifically, MSNs infected with Ltv-SCR had a rectification index larger than 1 indicating some degree of baseline rectification of the AMPAR-mediated outward currents in these cells. This is likely due to the presence of GluA2-containing AMPA receptors, which are blocked by intracellular polyamines at depolarized potentials (Man, 2011; Wolf and Tseng, 2012). Interestingly, MSNs infected with Ltv-shProsapip1 showed no evidence of outward rectification,

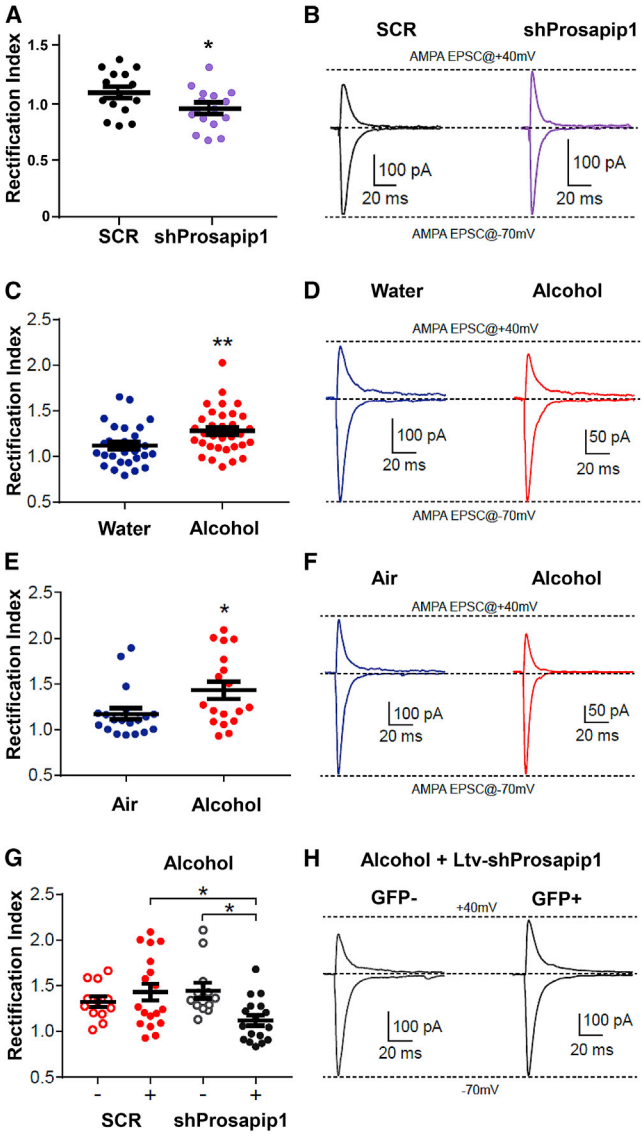

Figure 5. Prosapip1 Is Required for Alcohol-Dependent Change in AMPAR Subunit Composition at Glutamate Synapses

(A and B) The NAc of mice were infected bilaterally with Ltv-shProsapip1 or Ltv-SCR (1×10^8 pg/mL). Twenty-one days after virus administration, NAc slices were prepared and infected MSNs were patched. Electrically evoked AMPAR-mediated EPSCs were recorded from MSNs in the NAc shell at +40 mV and −70 mV from each group and rectification index was calculated. (A) The averages ± SEM of the rectification index are plotted for each group with symbols showing the values from individual cells. shProsapip1 (purple) 0.93 ± 0.05, SCR (black) 1.08 ± 0.05; significance difference was determined using two-tailed unpaired t test. $t_{(29)} = 2.194$, p = 0.036, n = 16 cells/4 mice (shProsapip1) and 15 cells/4 mice (shSCR). *p < 0.05. (B) Representative traces of AMPAR-mediated EPSC recorded at +40 mV and at −70 mV. The dotted lines show the expected amplitude for non-rectifying AMPAR-mediated currents.

(C and D) Mice underwent at least 8 weeks of IA20%-2BC. Mice consuming water only were used as control. Electrically evoked AMPAR-mediated EPSCs were recorded from MSNs in the NAc shell at +40 mV and −70 mV. (C) The averages ± SEM of the rectification index were plotted for each group with symbols showing the values from individual cells. Water (blue) 1.12 ± 0.04, alcohol (red) 1.28 ± 0.04; significance was determined using two-tailed unpaired t test. $t_{(59)} = 2.693$, p = 0.009, n = 28 cells/6 mice (water) and n = 33 cells/6 mice (alcohol). (D) Representative traces of AMPAR-mediated EPSCs recorded at +40 mV and −70 mV of MSNs from water (blue) or alcohol (red) group. Dotted lines depict the expected amplitude for non-rectifying AMPAR-mediated currents.

(E and F) The NAc of mice were infected bilaterally with Ltv-SCR. 21 days after virus administration, mice underwent 2 weeks of CIE exposure to alcohol vapor or air. Electrically evoked AMPAR-mediated EPSCs were recorded from GFP-positive MSNs expressing Ltv-SCR. (E) The averages ± SEM of the rectification index are plotted for each group with symbols showing the values from individual cells. Air (blue) 1.17 ± 0.06, CIE (red) 1.43 ± 0.09; Significance difference was determined using two-tailed unpaired t test. $t_{(35)} = 2.349$, p = 0.025, n = 19 cells/4 mice (air) and 18 cells/4 mice (CIE). (F) Representative traces of AMPAR-mediated EPSC recorded at +40 mV and at −70 mV. Dotted lines depict the expected amplitude for non-rectifying AMPAR-mediated currents. (G and H) The NAc of mice were infected bilaterally with Ltv-SCR or Ltv-shProsapip1. Twenty-one days after virus administration, mice underwent 2 weeks of CIE exposure to alcohol. Electrically evoked AMPAR-mediated EPSCs were recorded from GFP-negative (uninfected) or -positive (infected) MSNs from each group.

(G) The averages ± SEM of the rectification index are plotted for each group with symbols showing the values from individual cells. Ltv-SCR uninfected (red, empty) 1.327 ± 0.058, Ltv-SCR infected (red, filled) 1.432 ± 0.093, Ltv-shProsapip1 uninfected (gray, empty) 1.449 ± 0.086, Ltv-shProsapip1 (black, filled) 1.124 ± 0.058; one-way ANOVA indicates significant difference among means. F(3, 55) = 3.991, p = 0.012. *Post hoc* multiple comparison indicates significant difference between Ltv-SCR infected versus Ltv-shProsapip1 infected, p = 0.019; Ltv-shProsapip1 uninfected versus Ltv-shProsapip1 infected, p = 0.028. n = 12 cells (GFP−), 18 cells (GFP+)/4 mice (SCR) and 12 cells (GFP−), 16 cells (GFP+)/4 mice (shProsapip1).

(H) Representative traces of AMPAR-mediated EPSC recorded at +40 mV and at −70 mV. Dotted lines depict the expected amplitude for non-rectifying AMPAR-mediated currents. *p < 0.05, **p < 0.01.

suggesting a lower proportion of GluA2-lacking AMPA receptors (AMPARs) at the synapses. We also recorded miniature EPSCs and found no difference in the frequency of the events (Figures S7C and S7E), suggesting that there is no significant change in presynaptic properties of glutamate transmission. Finally, no change in mEPSC amplitude was detected (Figures S7D and S7E). Taken together, these data suggest that Prosapip1 is important for the synaptic localization of GluA2-lacking, calcium-permeable, AMPARs (Man, 2011).

We then we hypothesized that the consequences of alcohol-dependent Prosapip1 translation is the increase in membranal GluA2-lacking AMPARs. First, we tested whether alcohol intake increases the rectification index in the NAc shell in mice that underwent at least 8 weeks of IA20%-2BC reaching an average of 14.7 ± 0.9 g/kg/24 hr. We found that the rectification index was higher in NAc MSNs of alcohol-consuming animals compared to water-only-consuming mice (Figures 5C and 5D). Next, we examined the potential role of Prosapip1 in alcohol-dependent elevation of the rectification index. To do so, we used the non-contingent CIE paradigm in which mice undergo an intermittent exposure to alcohol vapor. First, mice were bilaterally infected with Ltv-SCR and recordings were made from NAc shell MSNs of alcohol or air exposed mice. As shown in Figures 5E and 5F, chronic vapor alcohol exposure produced an increase in the rectification index in the NAc shell MSNs of mice infected with Ltv-SCR as compared to air exposed controls infected with Ltv-SCR. Together these data indicate that alcohol increases the rectification index in the Nac shell, suggesting that a greater portion of

GluA2-lacking AMPARs are localized at the membrane. Next, we tested the rectification index in mice that underwent the CIE paradigm and were infected with either Ltv-shProsapip1 or Ltv-SCR. As shown in Figures 5G and 5H, the rectification index measured from NAc shell MSNs expressing Ltv-shProsapip1 was significantly lower compared to the rectification index measured in MSNs expressing Ltv-SCR. Furthermore, in the same animals infected with Ltv-shProsapip1, neighboring uninfected MSNs had high rectification index similar to Ltv-SCR (Figures 5G and 5H). Taken together, these data suggest that alcohol induces a membranal insertion of GluA2 lacking AMPARs at glutamatergic synapses, which is mediated by Prosapip1.

Prosapip1 in the NAc Contributes to Alcohol Self-Administration and Reward

Finally, we determined whether the Prosapip1-dependent cellular adaptations in the NAc described above contribute to mechanisms underlying alcohol-drinking behaviors. Mice underwent an IA20%-2BC for 7 weeks and were then trained to press on an active lever under fixed ratio 2 (FR2) schedule to obtain 20% alcohol (Figure S8). After establishing a stable baseline, the NAc of mice was infused with Ltv-shProsapip1 or Ltv-SCR, and alcohol self-administration was resumed after 2 weeks of recovery (Figure 6A). As shown in Figure 6, downregulation of Prosapip1 in the NAc produced a robust reduction in alcohol self-administration as evidenced by the reduction in number and frequency of active lever presses (Figures 6B–6D, Figure S8F), which corresponded with a reduction in the number of port entries (Figures 6E–6G) and in the amount of alcohol consumed (Figures 6H–6J). In addition, downregulation of Prosapip1 in the NAc increased the latency of the first active press and alcohol delivery (Figures 6K–6M), indicating a delay in the initiation of the alcohol self-administration episode, although the latency to the first port entry was not different between the two groups. Finally, Prosapip1 knockdown did not affect the latency of last active press or alcohol delivery (data not shown), suggesting an intact termination of the alcohol self-administration episode. In contrast to alcohol, downregulation of Prosapip1 levels did not alter lever presses for sucrose (Figure 6N). Specifically, knockdown of Prosapip1 did not alter the number of port entries (Figure 6O) or the amount of sucrose consumed (Figure 6P), indicating preserved operant responding for non-alcohol reward. Together, these data suggest that Prosapip1 in the NAc plays a specific role in alcohol self-administration.

Alcohol self-administration greatly depends upon the appetitive value of the reward, a process that critically involves the NAc (Floresco, 2015). Therefore, we postulated that Prosapip1 in the NAc contributes to alcohol reward processing. To test this hypothesis, mice infected with Ltv-shProsapip1 or Ltv-SCR in the NAc underwent a conditioned place preference (CPP) test in which alcohol administration is paired with a specific compartment (Figure 7A). During the preconditioning phase, the Ltv-shProsapip1 and Ltv-SCR groups did not differ in the distance traveled in the CPP apparatus (Figure 7B), indicating that Prosapip1 does not influence ambulatory activity. As shown in Figure 7C, alcohol place preference was detected in mice infected with Ltv-SCR but was attenuated in mice infected with Ltv-Prosapip1. In contrast, Prosapip1 knockdown had no effect on conditioned place aversion (CPA) to lithium chloride (Figures 7D and 7E), indicating that the ability to form conditioned associations was not impaired. Together, these data suggest that Prosapip1 in the NAc contributes to mechanisms underlying reward.

DISCUSSION

Our results point to Prosapip1 in the NAc as a critical component of alcohol-dependent cellular adaptations that promote alcohol-reward-related behaviors including alcohol seeking and drinking. Specifically, we show that alcohol-dependent activation of the mTORC1 signaling pathway in the NAc initiates the translation of Prosapip1. Prosapip1 then promotes the formation of actin filaments. Similarly, excessive alcohol drinking, by increasing Prosapip1 levels, promotes the formation of F-actin. The change in actin dynamics by alcohol produces morphological alterations of dendritic spines, which depend on Prosapip1. We further show that Prosapip1 in the NAc is required for the alcohol-dependent increase in the synaptic localization of GluA2-lacking calcium-permeable AMPARs. Finally, our data suggest that these molecular and cellular adaptations contribute to mechanisms that drive alcohol self-administration and reward.

RNA Sequencing Analysis

Prosapip1 was identified by a high-throughput RNA-seq approach as one of 12 mRNAs whose translation was increased by alcohol in an mTORC1-dependent manner. mTORC1 is best known for its role in the initiation of the translational machinery at dendrites (Buffington et al., 2014). Since polysomes were isolated from whole-cell lysates, we cannot exclude the possibility that the translation in response to alcohol occurs in cell bodies in addition to, or instead of, local translation at dendrites. mTORC1 initiates the translation of transcripts consisting of a 5′ terminal oligopyrimidine motif (TOP) or TOP-like motifs (Thoreen et al., 2012). Curiously, however, out of the 12 identified transcripts, only *RasGRP4* mRNA sequence contains a TOP-like motif (data not shown). However, recent studies suggest that the regulation of mRNA translation by mTORC1 signaling is not limited to TOP and TOP-like sequences (Gandin et al., 2016; Morita et al., 2013). Interestingly, three candidates are related to the microRNA (miRNA) gene-silencing machinery. Specifically, we found that Cnot4, a member of the Ccr4-Not complex that associates with RISC (Collart and Panasenko, 2012), the trinucleotide repeat containing 6a (Tnrc6a, also called GW182), a binding partner of Argonaute (Pfaff et al., 2013), and the trans-lin-associated factor X (Tsnax), which facilitates miRNA loading on RISC (Zhang et al., 2016), were enriched in the NAc polysomal fraction of alcohol-drinking mice but not in alcohol-consuming mice pre-treated with rapamycin. As mTORC1 has recently been shown to play a role in the regulation of miRNA production (Jewell et al., 2015), it would be of interest to assess the consequences of the increased translation of these targets by alcohol.

Prosapip1 and SPAR Signaling

We chose to focus our study on the role of the PSD protein Prosapip1 (Reim et al., 2016; Wendholt et al., 2006). Our studies reveal that, in addition to being a new downstream target of mTORC1, Prosapip1 controls actin dynamics, and by doing so,

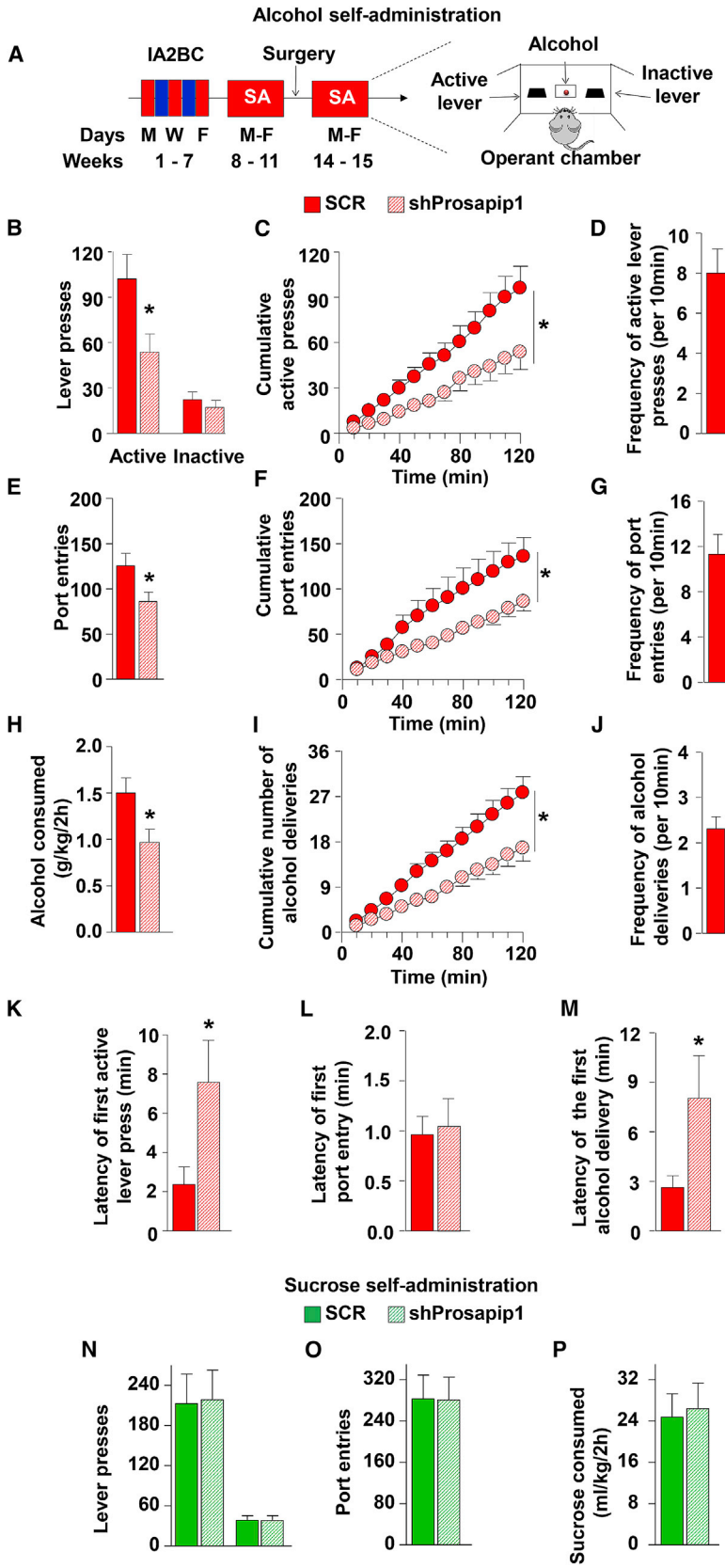

Figure 6. Prosapip1 in the NAc Drives Alcohol Self-Administration and Seeking

(A) Mice that underwent IA20%-2BC for 7–8 weeks were trained to self-administer 20% alcohol in operant chambers. After reaching a stable baseline of responding (see Figure S7), mice received an infusion of Ltv-SCR or Ltv-shProsapip1 in the NAc. Following 2 weeks of recovery, self-administration of alcohol was resumed for an additional 2 weeks.

(B) Number of active and inactive lever presses on the last self-administration session. shProsapip1 reduces the number of active ($t_{(18)}$ = 2.43, p = 0.026) but not inactive ($t_{(18)}$ = 0.73, p = 0.47) lever presses.

(C) Cumulative number of active lever presses. Two-way ANOVA indicates a significant main effect of shProsapip1 ($F_{(1,18)}$ = 5.67, p < 0.05) on cumulative number of active lever presses.

(D) Frequency of active lever presses. shProsapip1 reduces the frequency of active lever presses ($t_{(18)}$ = 2.25, p = 0.038).

(E) Number of port entries. shProsapip1 reduces the number of port entries ($t_{(18)}$ = 2.32, p = 0.033).

(F) Cumulative number of port entries. Two-way ANOVA indicates a significant main effect of shProsapip1 on cumulative number of port entries ($F_{(1,18)}$ = 4.04, p = 0.05).

(G) Frequency of port entries. shProsapip1 reduces the frequency of port entries ($t_{(18)}$ = 2.10, p = 0.05).

(H) Alcohol intake (g/kg/2 hr). shProsapip1 reduces the amount of alcohol consumed ($t_{(18)}$ = 2.45, p = 0.025).

(I) Cumulative number of alcohol deliveries. Two-way ANOVA indicates a significant main effect of shProsapip1 on cumulative number of alcohol deliveries ($F_{(1,18)}$ = 8.79, p < 0.05).

(J) Frequency of alcohol delivery. shProsapip1 reduces the frequency of alcohol delivery ($t_{(18)}$ = 2.67, p = 0.016).

(K) Latency of first active lever press. shProsapip1 increases the latency of first active lever press ($t_{(18)}$ = 2.24, p = 0.038).

(L) Latency of the first port entry. shProsapip1 does not affect the latency of first port entry ($t_{(18)}$ = 0.25, p = 0.81).

(M) Latency of the first alcohol delivery (min). shProsapip1 increases the latency of first alcohol delivery ($t_{(18)}$ = 2.02, p = 0.05).

(N–P) An independent cohort of mice was trained to self-administer 1% sucrose (see Figure S7) and received an infusion of Ltv-SCR or Ltv-shProsapip1 in the NAc.

(N) Number of active and inactive lever presses on the last self-administration session. shProsapip1 did not affect the number of active ($t_{(26)}$ = 0.09, p = 0.92) or inactive ($t_{(26)}$ = 0.04, p = 0.97) lever presses. (O) Number of port entries. shProsapip1 did not affect the number of port entries ($t_{(26)}$ = 0.03, p = 0.97). (P) Sucrose intake (mL/kg/2 hrs). shProsapip1 did not affect the amount of sucrose self-administered ($t_{(26)}$ = 0.24, p = 0.81). Data are represented as the average ± SEM (B–M) n = 10 per group and (N–P) n = 14 per group. *p < 0.05 versus SCR group.

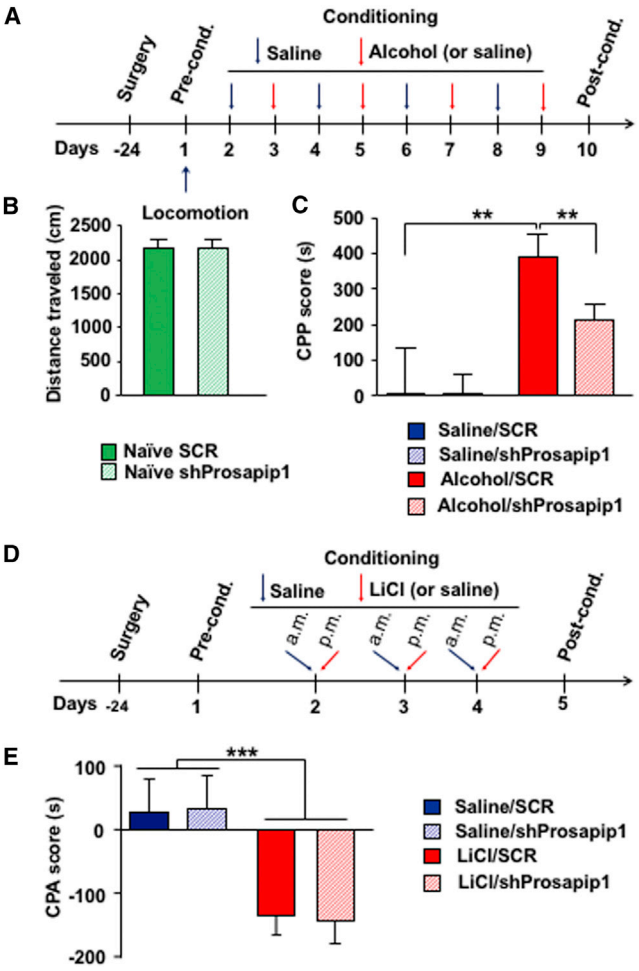

Figure 7. Prosapip1 in the NAc Contributes to Alcohol Reward

(A) Four weeks after intra-NAc administration of Ltv-shProsapip1 or SCR, mice underwent a CPP experiment in which they were daily administered (intraperitoneum, i.p.) with alcohol (1.8 g/kg) or saline prior to the confinement in the drug- or non-drug-paired compartment for 5 min. Following conditioning (8 days), a 15 min post-conditioning test was conducted.

(B) Distance traveled (cm) in the CPP apparatus prior to the conditioning phase. shProsapip1 does not alter ambulatory activity ($t_{(31)}$ = 0.01, p = 0.99). n = 15–18 per group.

(C) CPP score is expressed as the time (s) spent in the drug-paired compartment during the post-conditioning minus the time spent in the same compartment during the pre-conditioning period. Two-way ANOVA showed a main effect of conditioning (saline or alcohol; $F_{(1,31)}$ = 16.32, p < 0.001) and no interaction between conditioning and virus treatment ($F_{(1,31)}$ = 1.51, p = 0.23). Post hoc Student-Newman Keuls testing detected a significant difference between saline and alcohol in the scramble group (Saline/SCR versus Alcohol/SCR, p < 0.01) and a significant difference between animals who received shProsapip1 or scramble in the alcohol group (Alcohol/SCR versus Alcohol/shProsapip1, p < 0.01). n=7–10 per group.

(D) Four weeks after intra-NAc administration of Ltv-shProsapip1 or Ltv-SCR, mice underwent a CPA experiment in which they were administered daily (s.c.) with lithium chloride (LiCl, 130 mg/kg) or saline prior to confinement in the drug- or non-drug paired compartment for 45 min. Following conditioning (3 days, two sessions per day), a 20 min post-conditioning test was conducted.

(E) CPA score is expressed as the time (s) spent in the drug-paired compartment during post-conditioning minus the time spent in the same compartment during pre-conditioning. Two-way ANOVA showed a main effect of conditioning (saline or LiCl; $F_{(1, 26)}$ = 15.17, p = 0.0006), no effect of virus treatment ($F_{(1,26)}$ = 0.002, p = 0.963), and no interaction between virus and LiCl ($F_{(1,26)}$ = 0.024, p = 0.877). Further analysis by the method of contrast reveals a significant difference for the LiCl/SCR group and LiCl/shProsapip1 versus Saline/SCR group (respectively, p < 0.05) but no significant difference between LiCl/SCR and LiCl/shProsapip1 group (p = 0.99). Data are represented as the average ± SEM (B and C) n = 7–10 per group and (E) n = 7–8 per group. *p < 0.05 and ***p < 0.001.

the protein promotes the formation of mature mushroom-type spines in the NAc. Our results also suggest that Prosapip1 controls the synaptic membranal distribution of AMPAR subunits. It is plausible that Prosapip1 exerts these functions at least in part through Rap/SPAR signaling. Rap is a small G protein that promotes AMPARs internalization (Xie et al., 2005; Zhu et al., 2002, 2005). Rap2 produces spine loss and reduces the complexity of dendritic branching (Ryu et al., 2008; Xie et al., 2005), and Rap1 promotes the formation of thin spines (Xie et al., 2005). Rap activity is terminated by GAPs, which catalyzes the hydrolysis of GTP bound Rap to GDP (Bokoch, 1993). SPAR is the GAP for Rap in the brain (Spilker and Kreutz, 2010), and presumably by the termination of Rap activity, SPAR contributes to the increase in F-actin content in spines and to the enlargement of spine head (Maruoka et al., 2005; Pak et al., 2001). The mechanism by which SPAR promotes F-actin assembly is still unclear, and we demonstrate that Prosapip1 interacts with SPAR, and in parallel, promotes the formation of F-actin. This suggests that Prosapip1, potentially via the recruitment of SPAR to the PSD, may be the potential missing link between SPAR and F-Actin.

Interestingly, PSD-Zip70, another member of the Fezzin family that shares significant sequence homology with Prosapip1, interacts with SPAR to regulate the maturation of dendritic spines of cortical neurons (Maruoka et al., 2005). Whether PSD-Zip70 and Prosapip1 have restricted actions to specific brain regions or whether they interact together to regulate SPAR localization and F-actin dynamics in dendritic spines is an open question.

Prosapip1 and F-Actin-Dependent Mechanisms

We show that Prosapip1 contributes to two F-actin-dependent mechanisms: dendritic spine morphology (Cingolani and Goda, 2008), and surface composition of AMPARs subunits (Hanley, 2014). Synaptic strength is associated with morphological changes, particularly in the shape of dendritic spines, which are driven by reorganization of actin cytoskeleton (Cingolani and Goda, 2008). Thus, it is plausible that under normal physiological conditions, Prosapip1 plays a role in both structural and synaptic plasticity. This possibility should be further explored.

The Prosapip1/Actin Axis and Alcohol-Dependent Neuroadaptations

We found that alcohol-dependent activation of mTORC1 in the NAc increases the translation of Prosapip1. We show that the consequence of alcohol-dependent increase in Prosapip1 levels is the formation of actin filaments. Actin dynamics have been shown to be influenced by drugs of abuse. Specifically, actin polymerization promotes morphine place preference (Li et al., 2015), and reinstatement of methamphetamine and cocaine seeking (Young et al., 2014) in rodents. We show that excessive

alcohol consumption increases the F-actin content in the NAc of mice, which is mediated through Prosapip1. As mTORC1 is activated by numerous drugs of abuse (Neasta et al., 2014), it is plausible that the mTORC1/Prosapip1 axis is a master regulator of drug-dependent actin dynamics.

Actin polymerization contributes to dendritic spine morphology (Cingolani and Goda, 2008), as well as to the membranal insertion of GluA2-lacking AMPAR (Hanley, 2014), and we found that alcohol exposure produces alterations of both processes through Prosapip1. Specifically, we show that chronic alcohol intake as well as passive alcohol exposure produce an increase in the rectification index of the AMPAR-mediated outward currents in NAc shell MSNs. These findings are in line with recent studies suggesting that contingent and non-contingent alcohol administration increase the rectification index in NAc MSNs (Beckley et al., 2016; Renteria et al., 2017). Importantly, our data suggest that Prosapip1 controls this synaptic modification. Interestingly, exposure to cocaine and morphine triggers a switch in AMPAR subunit composition at NAc synapses (Hearing et al., 2016; McCutcheon et al., 2011). Thus, it is plausible that mTORC1 is the molecular driving force of synaptic plasticity induced by exposure to various drugs of abuse.

We found that alcohol drinking increased the average of spine area as well as the proportion of mature mushroom-type spines at the expense of thin immature spines in NAc shell MSNs and our data suggest that these alcohol-mediated morphological changes depend on Prosapip1. Interestingly, the translation of collapsine response mediator protein 2 (CRMP-2) is also increased in the NAc in response to alcohol intake in an mTORC1-dependent manner (Liu et al., 2017). The consequence of mTORC1-dependent translation of CRMP-2 by alcohol is the induction of microtubules assembly (Liu et al., 2017). Microtubules are present in dendritic shafts and the infiltration of microtubules into dendritic spines is correlated with increased F-actin and spine enlargement (Shirao and González-Billault, 2013). Thus, we postulate that alcohol via the activation of mTORC1 in the NAc produces orchestrated alterations of both microtubules and actin dynamics at the spines that lead to changes in synaptic strength that alter the landscape of the neuronal structure in response to excessive alcohol use.

Alcohol and Dendritic Spine Morphology

Interestingly, alcohol exposure produces different alterations in dendritic morphology in striatal subregions. For instance, we previously showed that excessive alcohol drinking increases dendritic branch length in D1R MSNs in the DMS (Wang et al., 2015), a change that we did not observe in the NAc shell of alcohol-drinking mice. In addition, and in contrast to the data presented herein, Uys et al. recently reported that chronic exposure to alcohol vapor increases the number of thin, stubby, and filopodia spines in the NAc core, and that 72 hours of withdrawal from CIE produced a reduction in the number of mushroom-type spines (Uys et al., 2016). However, also in contrast to Uys et al. findings and ours, Spiga et al. reported that alcohol-dependent rats undergoing withdrawal exhibit loss of thin spines in the NAc core, without alteration of mushroom-like spines (Spiga et al., 2014). We found that mTORC1 activation is localized to the NAc shell and is not observed in the NAc core or the DMS (Laguesse et al., 2016). The three striatal regions participate differentially in the mechanisms underlying alcohol seeking (Corbit et al., 2012, 2016). Thus, it is plausible that the mTORC1/Prosapip1 pathway participates specifically in mechanisms that drive the maturation of spines and the enlargement of spine heads in the NAc shell. Finally, it is important to note that the paradigm used in Spiga et al. and in the study presented here model two very different stages of alcohol use disorders (AUDs). The paradigm used in this study models "problem drinkers" in which subjects show high level of alcohol craving, seeking, and consumption (Enoch and Goldman, 2002), whereas Spiga et al.'s paradigm models a subset of problem drinkers in which individuals are physically dependent on alcohol (World Health Organization, 2004).

Prosapip1 and Alcohol-Dependent Behaviors

Given the importance of the NAc in reward-related behaviors (Baik, 2013; Volkow and Morales, 2015), and given the fact that drugs of abuse produce long-term synaptic and structural alterations in the brain (Russo et al., 2010), we tested the contribution of Prosapip1 in the NAc to alcohol seeking, drinking, and reward. Our findings suggest that Prosapip1 in the NAc participates in mechanisms that underlie the reinforcing and rewarding effects of alcohol. Alcohol self-administration, seeking, and place preference are learned behaviors that greatly depend on the ability of the animal to remember/retrieve associations (i.e., active lever-alcohol delivery and compartment-alcohol effect associations, respectively) (Huston et al., 2013). This raises the question of whether Prosapip1 influences the memory/retrieval of these associations. We found that Prosapip1 knockdown in the NAc did not affect the ability of the mice to differentiate between the active and inactive levers (i.e., discrimination ratio; Figure S8D) or acquire CPA for lithium chloride, which shows that that the ability to form conditioned associations has been preserved. Importantly, operant responding for the natural reward sucrose was not affected by Prosapip1 knockdown. This demonstrates that the consequences of Prosapip1-dependent events are selective for alcohol, and not generalizing to other goal-oriented behaviors. Together, our data imply that Prosapip1 promotes alcohol reward-related motivation to seek and consume alcohol.

Conclusion

In summary, we identified a new molecular axis composed of mTORC1, and its downstream mediator Prosapip1 that drives actin cytoskeleton reorganization as well as morphological and synaptic alteration at the dendritic spine level of NAc MSNs. Our results further suggest that this signaling pathway plays an important role in alcohol-dependent cellular adaptations that in turn enhance the rewarding effects of alcohol and promote alcohol-related behaviors such as alcohol drinking and seeking.

STAR★METHODS

Detailed methods are provided in the online version of this paper and include the following:

- KEY RESOURCES TABLE
- CONTACT FOR REAGENT AND RESOURCE SHARING

SUPPLEMENTAL INFORMATION

Supplemental Information includes eight figures and can be found with this article online at http://dx.doi.org/10.1016/j.neuron.2017.08.037.

AUTHOR CONTRIBUTIONS

Conceptualization, S.L. and D.R.; Methodology, S.L. and D.R.; Investigation, S.L., N.M., S.A.S., F.L., M.F.A., J.H.S.; Validation, S.L., N.M., S.A.S., F.L., J.H.S., M.F.A., and M.F.L.; Analysis, S.L., N.M., S.A.S., J.H.S., V.A.A., and K.J.B.; Data Curation, S.L. and D.R.; Visualization, S.L. and N.M.; Resources, K.P., H.C.B., and W.C.G.; Writing-original draft S.L. and D.R.; Writing-Review & Editing, D.R., S.L., S.A.S., and V.A.A.; Funding acquisition, D.R.; Supervision, D.R., K.J.B., and V.A.A.

ACKNOWLEDGMENTS

We thank Dr. Daniel Pak Georgetown University for sharing the HA-SPAR plasmid and Ms. Dana Renae Kennedy for her help in dendritic spine analysis. This research was supported by the NIAAA, P50AA017072 (D.R.), P50AA010761 (H.C.B.), ZIA-AA000421 (V.A.A.), and the Belgian American Education Foundation (S.L.).

Received: February 2, 2017
Revised: June 13, 2017
Accepted: August 24, 2017
Published: September 7, 2017

REFERENCES

Baik, J.H. (2013). Dopamine signaling in reward-related behaviors. Front. Neural Circuits *7*, 152.

Barak, S., Liu, F., Ben Hamida, S., Yowell, Q.V., Neasta, J., Kharazia, V., Janak, P.H., and Ron, D. (2013). Disruption of alcohol-related memories by mTORC1 inhibition prevents relapse. Nat. Neurosci. *16*, 1111–1117.

Becker, H.C., and Lopez, M.F. (2004). Increased ethanol drinking after repeated chronic ethanol exposure and withdrawal experience in C57BL/6 mice. Alcohol. Clin. Exp. Res. *28*, 1829–1838.

Beckley, J.T., Laguesse, S., Phamluong, K., Morisot, N., Wegner, S.A., and Ron, D. (2016). The First Alcohol Drink Triggers mTORC1-Dependent Synaptic Plasticity in Nucleus Accumbens Dopamine D1 Receptor Neurons. J. Neurosci. *36*, 701–713.

Ben Hamida, S., Neasta, J., Lasek, A.W., Kharazia, V., Zou, M., Carnicella, S., Janak, P.H., and Ron, D. (2012). The small G protein H-Ras in the mesolimbic system is a molecular gateway to alcohol-seeking and excessive drinking behaviors. J. Neurosci. *32*, 15849–15858.

Bokoch, G.M. (1993). Biology of the Rap proteins, members of the ras superfamily of GTP-binding proteins. Biochem. J. *289*, 17–24.

Buffington, S.A., Huang, W., and Costa-Mattioli, M. (2014). Translational control in synaptic plasticity and cognitive dysfunction. Annu. Rev. Neurosci. *37*, 17–38.

Cingolani, L.A., and Goda, Y. (2008). Actin in action: the interplay between the actin cytoskeleton and synaptic efficacy. Nat. Rev. Neurosci. *9*, 344–356.

Collart, M.A., and Panasenko, O.O. (2012). The Ccr4–not complex. Gene *492*, 42–53.

Corbit, L.H., Nie, H., and Janak, P.H. (2012). Habitual alcohol seeking: time course and the contribution of subregions of the dorsal striatum. Biol. Psychiatry *72*, 389–395.

Corbit, L.H., Fischbach, S.C., and Janak, P.H. (2016). Nucleus accumbens core and shell are differentially involved in general and outcome-specific forms of Pavlovian-instrumental transfer with alcohol and sucrose rewards. Eur. J. Neurosci. *43*, 1229–1236.

del Prete, M.J., Vernal, R., Dolznig, H., Müllner, E.W., and Garcia-Sanz, J.A. (2007). Isolation of polysome-bound mRNA from solid tissues amenable for RT-PCR and profiling experiments. RNA *13*, 414–421.

Enoch, M.A., and Goldman, D. (2002). Problem drinking and alcoholism: diagnosis and treatment. Am. Fam. Physician *65*, 441–448.

Fischer, C., Christ, E., Korf, H.W., and von Gall, C. (2012). Tafa-3 encoding for a secretory peptide is expressed in the mouse pars tuberalis and is affected by melatonin 1 receptor deficiency. Gen. Comp. Endocrinol. *177*, 98–103.

Floresco, S.B. (2015). The nucleus accumbens: an interface between cognition, emotion, and action. Annu. Rev. Psychol. *66*, 25–52.

Gandin, V., Masvidal, L., Hulea, L., Gravel, S.P., Cargnello, M., McLaughlan, S., Cai, Y., Balanathan, P., Morita, M., Rajakumar, A., et al. (2016). nanoCAGE reveals 5′ UTR features that define specific modes of translation of functionally related MTOR-sensitive mRNAs. Genome Res. *26*, 636–648.

Gentry, R.T., and Dole, V.P. (1987). Why does a sucrose choice reduce the consumption of alcohol in C57BL/6J mice? Life Sci. *40*, 2191–2194.

Griffin, W.C., 3rd, Lopez, M.F., and Becker, H.C. (2009). Intensity and duration of chronic ethanol exposure is critical for subsequent escalation of voluntary ethanol drinking in mice. Alcohol. Clin. Exp. Res. *33*, 1893–1900.

Hanley, J.G. (2014). Actin-dependent mechanisms in AMPA receptor trafficking. Front. Cell. Neurosci. *8*, 381.

Hearing, M.C., Jedynak, J., Ebner, S.R., Ingebretson, A., Asp, A.J., Fischer, R.A., Schmidt, C., Larson, E.B., and Thomas, M.J. (2016). Reversal of morphine-induced cell-type-specific synaptic plasticity in the nucleus accumbens shell blocks reinstatement. Proc. Natl. Acad. Sci. USA *113*, 757–762.

Hering, H., and Sheng, M. (2001). Dendritic spines: structure, dynamics and regulation. Nat. Rev. Neurosci. *2*, 880–888.

Hotulainen, P., and Hoogenraad, C.C. (2010). Actin in dendritic spines: connecting dynamics to function. J. Cell Biol. *189*, 619–629.

Huang, W., Zhu, P.J., Zhang, S., Zhou, H., Stoica, L., Galiano, M., Krnjević, K., Roman, G., and Costa-Mattioli, M. (2013). mTORC2 controls actin polymerization required for consolidation of long-term memory. Nat. Neurosci. *16*, 441–448.

Huston, J.P., Silva, M.A., Topic, B., and Müller, C.P. (2013). What's conditioned in conditioned place preference? Trends Pharmacol. Sci. *34*, 162–166.

Hwa, L.S., Chu, A., Levinson, S.A., Kayyali, T.M., DeBold, J.F., and Miczek, K.A. (2011). Persistent escalation of alcohol drinking in C57BL/6J mice with intermittent access to 20% ethanol. Alcohol. Clin. Exp. Res. *35*, 1938–1947.

Hyman, S.E. (2005). Addiction: a disease of learning and memory. Am. J. Psychiatry *162*, 1414–1422.

Jewell, J.L., Flores, F., and Guan, K.L. (2015). Micro(RNA) managing by mTORC1. Mol. Cell *57*, 575–576.

Kasai, H., Matsuzaki, M., Noguchi, J., Yasumatsu, N., and Nakahara, H. (2003). Structure-stability-function relationships of dendritic spines. Trends Neurosci. *26*, 360–368.

Laguesse, S., Morisot, N., Phamluong, K., and Ron, D. (2016). Region specific activation of the AKT and mTORC1 pathway in response to excessive alcohol intake in rodents. Addict. Biol. Published online October 20, 2016. http://dx.doi.org/10.1111/adb.12464.

Lasek, A.W., Janak, P.H., He, L., Whistler, J.L., and Heberlein, U. (2007). Downregulation of mu opioid receptor by RNA interference in the ventral tegmental area reduces ethanol consumption in mice. Genes Brain Behav. *6*, 728–735.

Lee, K.W., Kim, Y., Kim, A.M., Helmin, K., Nairn, A.C., and Greengard, P. (2006). Cocaine-induced dendritic spine formation in D1 and D2 dopamine receptor-containing medium spiny neurons in nucleus accumbens. Proc. Natl. Acad. Sci. USA *103*, 3399–3404.

Legastelois, R., Darcq, E., Wegner, S.A., Lombroso, P.J., and Ron, D. (2015). Striatal-enriched protein tyrosine phosphatase controls responses to aversive stimuli: implication for ethanol drinking. PLoS ONE *10*, e0127408.

Li, Z., Wu, Y., and Baraban, J.M. (2008). The Translin/Trax RNA binding complex: clues to function in the nervous system. Biochim. Biophys. Acta *1779*, 479–485.

Li, J., Kim, S.G., and Blenis, J. (2014). Rapamycin: one drug, many effects. Cell Metab. *19*, 373–379.

Li, G., Wang, Y., Yan, M., Xu, Y., Song, X., Li, Q., Zhang, J., Ma, H., and Wu, Y. (2015). Inhibition of actin polymerization in the NAc shell inhibits morphine-induced CPP by disrupting its reconsolidation. Sci. Rep. *5*, 16283.

Liu, F., Laguesse, S., Legastelois, R., Morisot, N., Ben Hamida, S., and Ron, D. (2017). mTORC1-dependent translation of collapsin response mediator protein-2 drives neuroadaptations underlying excessive alcohol-drinking behaviors. Mol. Psychiatry *22*, 89–101.

Ma, X.M., and Blenis, J. (2009). Molecular mechanisms of mTOR-mediated translational control. Nat. Rev. Mol. Cell Biol. *10*, 307–318.

Man, H.Y. (2011). GluA2-lacking, calcium-permeable AMPA receptors–inducers of plasticity? Curr. Opin. Neurobiol. *21*, 291–298.

Maruoka, H., Konno, D., Hori, K., and Sobue, K. (2005). Collaboration of PSD-Zip70 with its binding partner, SPAR, in dendritic spine maturity. J. Neurosci. *25*, 1421–1430.

McCutcheon, J.E., Wang, X., Tseng, K.Y., Wolf, M.E., and Marinelli, M. (2011). Calcium-permeable AMPA receptors are present in nucleus accumbens synapses after prolonged withdrawal from cocaine self-administration but not experimenter-administered cocaine. J. Neurosci. *31*, 5737–5743.

Morisot, N., Novotny, C.J., Shokat, K.M., and Ron, D. (2017). A new generation of mTORC1 inhibitor attenuates alcohol intake and reward in mice. Addict Biol. Published online July 6, 2017. http://dx.doi.org/10.1111/adb.12528.

Morita, M., Gravel, S.P., Chénard, V., Sikström, K., Zheng, L., Alain, T., Gandin, V., Avizonis, D., Arguello, M., Zakaria, C., et al. (2013). mTORC1 controls mitochondrial activity and biogenesis through 4E-BP-dependent translational regulation. Cell Metab. *18*, 698–711.

Mortazavi, A., Williams, B.A., McCue, K., Schaeffer, L., and Wold, B. (2008). Mapping and quantifying mammalian transcriptomes by RNA-Seq. Nat. Methods *5*, 621–628.

Neasta, J., Ben Hamida, S., Yowell, Q., Carnicella, S., and Ron, D. (2010). Role for mammalian target of rapamycin complex 1 signaling in neuroadaptations underlying alcohol-related disorders. Proc. Natl. Acad. Sci. USA *107*, 20093–20098.

Neasta, J., Barak, S., Hamida, S.B., and Ron, D. (2014). mTOR complex 1: a key player in neuroadaptations induced by drugs of abuse. J. Neurochem. *130*, 172–184.

Pak, D.T., Yang, S., Rudolph-Correia, S., Kim, E., and Sheng, M. (2001). Regulation of dendritic spine morphology by SPAR, a PSD-95-associated RapGAP. Neuron *31*, 289–303.

Pfaff, J., Hennig, J., Herzog, F., Aebersold, R., Sattler, M., Niessing, D., and Meister, G. (2013). Structural features of Argonaute-GW182 protein interactions. Proc. Natl. Acad. Sci. USA *110*, E3770–E3779.

Potter, L.R. (2011). Guanylyl cyclase structure, function and regulation. Cell. Signal. *23*, 1921–1926.

Reim, D., Weis, T.M., Halbedl, S., Delling, J.P., Grabrucker, A.M., Boeckers, T.M., and Schmeisser, M.J. (2016). The Shank3 Interaction Partner ProSAPiP1 Regulates Postsynaptic SPAR Levels and the Maturation of Dendritic Spines in Hippocampal Neurons. Front. Synaptic Neurosci. *8*, 13.

Renteria, R., Buske, T.R., and Morrisett, R.A. (2017). Long-term subregion-specific encoding of enhanced ethanol intake by D1DR medium spiny neurons of the nucleus accumbens. Addict. Biol. Published online June 28, 2017. http://dx.doi.org/10.1111/adb.12526.

Russo, S.J., Dietz, D.M., Dumitriu, D., Morrison, J.H., Malenka, R.C., and Nestler, E.J. (2010). The addicted synapse: mechanisms of synaptic and structural plasticity in nucleus accumbens. Trends Neurosci. *33*, 267–276.

Ryu, J., Futai, K., Feliu, M., Weinberg, R., and Sheng, M. (2008). Constitutively active Rap2 transgenic mice display fewer dendritic spines, reduced extracellular signal-regulated kinase signaling, enhanced long-term depression, and impaired spatial learning and fear extinction. J. Neurosci. *28*, 8178–8188.

Shirao, T., and González-Billault, C. (2013). Actin filaments and microtubules in dendritic spines. J. Neurochem. *126*, 155–164.

Sholl, D.A. (1953). Dendritic organization in the neurons of the visual and motor cortices of the cat. J. Anat. *87*, 387–406.

Smith, D.L., Pozueta, J., Gong, B., Arancio, O., and Shelanski, M. (2009). Reversal of long-term dendritic spine alterations in Alzheimer disease models. Proc. Natl. Acad. Sci. USA *106*, 16877–16882.

Sonenberg, N., and Hinnebusch, A.G. (2009). Regulation of translation initiation in eukaryotes: mechanisms and biological targets. Cell *136*, 731–745.

Spiga, S., Talani, G., Mulas, G., Licheri, V., Fois, G.R., Muggironi, G., Masala, N., Cannizzaro, C., Biggio, G., Sanna, E., and Diana, M. (2014). Hampered long-term depression and thin spine loss in the nucleus accumbens of ethanol-dependent rats. Proc. Natl. Acad. Sci. USA *111*, E3745–E3754.

Spilker, C., and Kreutz, M.R. (2010). RapGAPs in brain: multipurpose players in neuronal Rap signalling. Eur. J. Neurosci. *32*, 1–9.

Thoreen, C.C., Chantranupong, L., Keys, H.R., Wang, T., Gray, N.S., and Sabatini, D.M. (2012). A unifying model for mTORC1-mediated regulation of mRNA translation. Nature *485*, 109–113.

Tom Tang, Y., Emtage, P., Funk, W.D., Hu, T., Arterburn, M., Park, E.E., and Rupp, F. (2004). TAFA: a novel secreted family with conserved cysteine residues and restricted expression in the brain. Genomics *83*, 727–734.

Trapnell, C., Pachter, L., and Salzberg, S.L. (2009). TopHat: discovering splice junctions with RNA-Seq. Bioinformatics *25*, 1105–1111.

Trapnell, C., Roberts, A., Goff, L., Pertea, G., Kim, D., Kelley, D.R., Pimentel, H., Salzberg, S.L., Rinn, J.L., and Pachter, L. (2012). Differential gene and transcript expression analysis of RNA-seq experiments with TopHat and Cufflinks. Nat. Protoc. *7*, 562–578.

Uys, J.D., McGuier, N.S., Gass, J.T., Griffin, W.C., 3rd, Ball, L.E., and Mulholland, P.J. (2016). Chronic intermittent ethanol exposure and withdrawal

leads to adaptations in nucleus accumbens core postsynaptic density proteome and dendritic spines. Addict. Biol. *21*, 560–574.

Volkow, N.D., and Morales, M. (2015). The Brain on Drugs: From Reward to Addiction. Cell *162*, 712–725.

Wang, Z., Gerstein, M., and Snyder, M. (2009). RNA-Seq: a revolutionary tool for transcriptomics. Nat. Rev. Genet. *10*, 57–63.

Wang, J., Lanfranco, M.F., Gibb, S.L., Yowell, Q.V., Carnicella, S., and Ron, D. (2010). Long-lasting adaptations of the NR2B-containing NMDA receptors in the dorsomedial striatum play a crucial role in alcohol consumption and relapse. J. Neurosci. *30*, 10187–10198.

Wang, J., Cheng, Y., Wang, X., Roltsch Hellard, E., Ma, T., Gil, H., Ben Hamida, S., and Ron, D. (2015). Alcohol Elicits Functional and Structural Plasticity Selectively in Dopamine D1 Receptor-Expressing Neurons of the Dorsomedial Striatum. J. Neurosci. *35*, 11634–11643.

Warnault, V., Darcq, E., Levine, A., Barak, S., and Ron, D. (2013). Chromatin remodeling–a novel strategy to control excessive alcohol drinking. Transl. Psychiatry *3*, e231.

Wendholt, D., Spilker, C., Schmitt, A., Dolnik, A., Smalla, K.H., Proepper, C., Bockmann, J., Sobue, K., Gundelfinger, E.D., Kreutz, M.R., and Boeckers, T.M. (2006). ProSAP-interacting protein 1 (ProSAPiP1), a novel protein of the postsynaptic density that links the spine-associated Rap-Gap (SPAR) to the scaffolding protein ProSAP2/Shank3. J. Biol. Chem. *281*, 13805–13816.

Wolf, M.E., and Tseng, K.Y. (2012). Calcium-permeable AMPA receptors in the VTA and nucleus accumbens after cocaine exposure: when, how, and why? Front. Mol. Neurosci. *5*, 72.

World Health Organization (2004). WHO Global Status Report on Alcohol 2004 (World Health Organization).

Xie, Z., Huganir, R.L., and Penzes, P. (2005). Activity-dependent dendritic spine structural plasticity is regulated by small GTPase Rap1 and its target AF-6. Neuron *48*, 605–618.

Young, E.J., Aceti, M., Griggs, E.M., Fuchs, R.A., Zigmond, Z., Rumbaugh, G., and Miller, C.A. (2014). Selective, retrieval-independent disruption of methamphetamine-associated memory by actin depolymerization. Biol. Psychiatry *75*, 96–104.

Zapata, A., Gonzales, R.A., and Shippenberg, T.S. (2006). Repeated ethanol intoxication induces behavioral sensitization in the absence of a sensitized accumbens dopamine response in C57BL/6J and DBA/2J mice. Neuropsychopharmacology *31*, 396–405.

Zhang, J., Liu, H., Yao, Q., Yu, X., Chen, Y., Cui, R., Wu, B., Zheng, L., Zuo, J., Huang, Z., et al. (2016). Structural basis for single-stranded RNA recognition and cleavage by C3PO. Nucleic Acids Res. *44*, 9494–9504.

Zhu, J.J., Qin, Y., Zhao, M., Van Aelst, L., and Malinow, R. (2002). Ras and Rap control AMPA receptor trafficking during synaptic plasticity. Cell *110*, 443–455.

Zhu, Y., Pak, D., Qin, Y., McCormack, S.G., Kim, M.J., Baumgart, J.P., Velamoor, V., Auberson, Y.P., Osten, P., van Aelst, L., et al. (2005). Rap2-JNK removes synaptic AMPA receptors during depotentiation. Neuron *46*, 905–916.

STAR★METHODS

KEY RESOURCES TABLE

REAGENT or RESOURCE	SOURCE	IDENTIFIER
Antibodies		
Rabbit polyclonal anti-phospho-4E-BP Thr37/46	Cell signaling technology	#2855S; RRID: AB_560835
Rabbit polyclonal anti-4E-BP	Cell signaling technology	#2845S; RRID: AB_10699019
Rabbit monoclonal anti-phospho-p70Kinase Thr389	Cell signaling technology	#9234S; RRID: AB_2269803
Rabbit monoclonal anti-p70Kinase	Cell signaling technology	#2708S; RRID: AB_390722
Rabbit anti-GAPDH	Santa Cruz Biotechnology	sc-25778; RRID: AB_10167668
Mouse monoclonal anti-HA	Santa Cruz Biotechnology	sc-7392; RRID: AB_627809
Rabbit polyclonal anti-Prosapip1	Proteintech	24936-1-AP
Rabbit polyclonal anti-SPAR (Sipa1L1)	Proteintech	25086-1-AP
Chicken polyclonal anti-GFP	Life Technologies	A10262; RRID: AB_2534023
Mouse monoclomal anti-NeuN	Millipore	MAB377; RRID: AB_2298772
Mouse monoclonal anti-actin	Sigma-Aldrich	A2228; RRID: AB_476697
Mouse monoclonal anti-flag	Sigma-Aldrich	F3165; RRID: AB_259529
Bacterial and Virus Strains		
LentiLox 3.7 (pLL3.7) lentivirus	Addgene, this paper	#11795
pLVX-IRES-GFP lentivirus	Clontech, this paper	632187
Chemicals, Peptides, and Recombinant Proteins		
sucrose	Sigma-Aldrich	S0389
saccharin	Sigma-Aldrich	109185
Ethyl alcohol	VWR	64-17-5
Lithium chloride	Santa Cruz Biotechnology	CAS 7447-41-8
Ribonucleoside vanadyl complex (RVC)	New England Biolabs	S1402S
Recombinant Rnasin Ribonuclease Inhibitor	Promega	N2515
Proteinase K	Promega	V3021
Rapamycin	LC Laboratories	R-5000
TRIzol	Life Technologies	15596026
EDTA-free complete mini Protease Inhibitor Cocktails	Sigma-Aldrich	11873580001
phosphatase inhibitor Cocktails 2	Sigma-Aldrich	P5726
phosphatase inhibitor Cocktails 3	Sigma-Aldrich	P0044
Protein A/G plus beads	Santa Cruz Biotechnology	sc-2003
SYBR Green PCR Master mix	Thermo Fisher Scientific	A25742
Critical Commercial Assays		
G-actin/F-actin *in vivo* assay biochem kit	Cytoskeleton	# BK037
Pierce bicinchoninic acid (BCA) protein assay kit	Thermo Fisher Scientific	23225
HIV-1 p24 antigen ELISA kit	ZeptoMetrix Corporation	0801111
Reverse Transcription System	Promega	A3500
Deposited Data		
Raw data associated with this paper	N/A	http://dx.doi.org/10.17632/xzmp3zffz7.1
Experimental Models: Cell Lines		
Neuro-2a	ATCC	CCL-131
Lenti-X 293T cells	Clontech	632180
Experimental Models: Organisms/Strains		
Mouse: C57BL/6J	The Jackson Laboratory	000664; RRID: IMSR_JAX:000664

(*Continued on next page*)

Continued

REAGENT or RESOURCE	SOURCE	IDENTIFIER
Oligonucleotides		
siRNA targeting sequence: Prosapip1: 5′-GGG AAG AGC TGG AGG ACA A-3′	This paper	N/A
Scrambled sequence: 5′-GCG CUU AGC UGU AGG AUU C-3′	This paper	N/A
Prosapip1 primers: 5′-GTC TGT CAG AAG GAG CAG GC-3′ and 5′-CCC CAC GAT CTC ACT CAA CT-3′	This paper	N/A
Gucy1a3 primers: 5′-CTT CCA CCA AAC TTC CCT A-3′ and 5′-GAA CCC ATT ACT TCA ACA CTT A-3′	This paper	N/A
TAFA-3 primers: 5′-AGA AGG TAA ATC AGC CAT AGT-3′ and 5′-ACA GAG GGT GAG CCA AGA-3′	This paper	N/A
Tsnax Primers: 5′-ATG TGC TCG CTC TAT TGT T-3′ and 5′-ATC GGT GAG AAA GGA AAA-3′	This paper	N/A
GAPDH primers: 5′-CGA CTT CAA CAG CAA CTC CCA CTC TTC C-3′ and 5′-TGG GTG GTC CAG GGT TTC TTA CTC CTT-3′	This paper	N/A
Recombinant DNA		
HA-SPAR	Gift from D. Pak, Georgetown University	N/A
Plvx-Prosapip1-IRES-GFP	This paper	N/A
pLL3.7 shProsapip1	Addgene, This paper	#11795
pLL3.7 SCR	Liu et al., 2017	#11795
Software and Algorithms		
TopHat, Cufflinks: Galaxy public server platform	Trapnell et al., 2009, 2012	http://galaxy.psu.edu/
ImageJ (NIH)	NIH	https://imagej.nih.gov/ij/
AutoQuant X3	Media Cybernetics	http://www.mediacy.com/

CONTACT FOR REAGENT AND RESOURCE SHARING

Further information and requests for resources and reagents should be directed to and will be fulfilled by the Lead Contact, Dorit Ron (dorit.ron@ucsf.edu).

EXPERIMENTAL MODEL AND SUBJECT DETAILS

Animals

Male C57BL/6J mice were purchased from Jackson Laboratory (Bar Harbor, ME). All the molecular and behavioral studies were performed at the University of California San Francisco (UCSF), and the electrophysiology experiments were conducted at the National Institute on Alcohol Abuse and Alcoholism (NIAAA). Chronic Intermittent vapor Exposure (CIE) to alcohol was done at the Medical University South Carolina (MUSC), and at NIAAA.

UCSF - Mice were 8-9 weeks old at the beginning of the experiments and were individually housed in temperature and humidity controlled rooms under a reversed 12-hours light/dark cycle (lights on at 22:00) or a 12-hours light/dark cycle (lights on at 07:00; CPP experiment only) with food and water available *ad libitum*. All animal procedures were approved by the University of California San Francisco (UCSF) Institutional Animal Care and Use Committee and were conducted in agreement with the Association for Assessment and Accreditation of Laboratory Animal Care (AAALAC, UCSF).

MUSC - Mice were 10-11 weeks old at the beginning of the study. Mice were individually housed in AAALAC accredited facilities with free access to food and water *ad libitum* throughout all phases of the experiments. Body weights were recorded daily during the chronic intermittent vapor alcohol (CIE) or air exposure. Mice were housed in a temperature and humidity-controlled animal facility under a reversed 12-hours light/dark cycle (lights on at 18:00). All procedures were approved by MUSC Institutional Animal Care and Use Committee and followed the NIH Guide for the Care and Use of Laboratory Animals (8^{th} edition, National Research Council, 2011).

NIAAA - Mice were 8-12 weeks old at the beginning of the study and were group housed in AAALAC accredited facility with food and water available *ad libitum*. Housing room has controlled temperature and humidity and is kept under a 12-hours light/dark cycle

(lights on at 06:30) or a reversed 12-hours light/dark cycle (lights on at 18:30; IA-2BC only). Mice were individually housed after surgery. All procedures were approved and performed in accordance with guidelines from the NIAAA Animal Care and Use Committee.

METHOD DETAILS

Cell culture and transfection

Murine neuroblastoma Neuro2A cells (ATCC, Manassas, VA) were maintained in Dulbecco's modified Eagle's medium DMEM H-21 (Sigma Aldrich) supplemented with 10% fetal bovine serum (FBS). Medium was removed and replaced by Opti-MEM (Sigma Aldrich) and transfection was performed using Lipofectamine 2000 according to the manufacturer's protocol (Invitrogen). After 4 hours, medium was replaced by DMEM-10% FBS. Forty-eight hours after transfection, cell differentiation was induced by replacing the medium with DMEM-1% FBS for another 48 hours.

Preparation of solutions

Alcohol solution was prepared from ethyl alcohol solution (95 proof) diluted to 20% (v/v) in tap water for the drinking experiments. Rapamycin was dissolved in DMSO and given systemically at a dose of 20 mg/kg or 40 mg/kg (Neasta et al., 2010). Lithium chloride was dissolved in saline 0.9% and given systemically at a dose of 130 mg/kg. Saccharin solution (0.01%) was prepared in tap water. Sucrose (1%) was dissolved in tap water (w/v).

Collection of brain samples for biochemical analyses

Mice that underwent the IA20%-2BC paradigm for 7-8 weeks were euthanized 4 hours after the beginning of the last drinking session (''binge'' time point) or 24 hours after the end of the last drinking session (''withdrawal'' time point). Afterward, brains were quickly removed and regions were dissected on an ice-cold platform.

Polysomal fractionation

Polysome-bound RNA was purified from mouse NAc according to (Liu et al., 2017). Specifically, fresh mouse NAc was snap-frozen in a 1.5 mL Eppendorf tube and pulverized in liquid nitrogen with a pestle. After keeping on dry ice for 5 min, the powder of one NAc was resuspended in 1 mL lysis buffer (10 mM Tris pH 8.0, 150 mM NaCl, 5 mM $MgCl_2$, 1% NP40, 0.5% sodium deoxycholate, 40 mM dithiothreitol, 400 U/mL Rnasin, 10 mM Ribonucleoside Vanadyl Complex and 200 μg/mL cycloheximide) followed by pipetting 20 times to further disrupt cell membranes. Two hundred μL of the homogenate was subjected to total RNA extraction using TRIzol reagent. The rest of the homogenate was centrifuged for 10 s at 12.000 g to remove intact nuclei. The supernatant was collected and ribosomes were further released by adding 2X extraction buffer (200mM Tris pH7.5, 300mM NaCl and 200μg/mL cycloheximide). Samples were kept on ice for 5 min and then centrifuged at 12.000 g, 4°C for 5 min to remove mitochondria and membranous debris. The resulting supernatant was loaded onto a 15%–45% sucrose gradient and centrifuged in a SW41Ti rotor (Beckman Coulter) at 38.000rpm, 4°C for 2 hours. Sucrose gradient fractions were collected and further digested with proteinase K (400μg/mL proteinase K, 10mM EDTA, 1% SDS) at 37°C for 30 min, followed by phenol-chloroform extraction. RNA in the water phase of the polysomal fraction was recovered by ethyl alcohol precipitation. The purity of the polysomal fractions was assessed by visualizing presence of 28S and 18S ribosomal RNA bands on an agarose gel and by measuring absorbance at 254 nm, as previously described (Liu et al., 2017).

RNA sequencing

RNA sequencing (RNA-seq) was conducted as described in (Wang et al., 2009). Four groups of animals (Water/Vehicle, Water/Rapamycin, Alcohol/Vehicle, Alcohol/Rapamycin), six animals per group were used to generate the RNA-seq data. Purified polysomal RNA from 2 mice NAc were pooled into 1 sample and made into 1 cDNA library using the TruSeq RNA Library Preparation kit v2 (Illumina). All the libraries were quantified, and the size and purity of each sample was determined by qPCR according to manufacturer's protocol. cDNA libraries from the 4 conditions were made with different RNA-adaptor indices. Four libraries (one per condition) were pooled into one lane for RNA-seq by Hiseq 2000 DNA sequencer (Illumina) in the Genomics Sequencing Laboratory at the University of California Berkeley and 3 lanes were sequenced. Each lane generated at least 8 Gb (180 million reads) raw compressed data, which was considered sufficient for in depth sequencing of 4 pooled libraries (Mortazavi et al., 2008). To perform differential analysis for changes in polysomal transcript expression, RNA-seq reads alignment and differential analysis were conducted using TopHat and Cufflinks on the Galaxy public server platform (http://galaxy.psu.edu/), as previously described (Trapnell et al., 2009; Trapnell et al., 2012). The following criteria were used for analysis: A cutoff of fold change > 1.5 was used for transcripts whose translation was increased in the ''Alcohol/Vehicle'' group compared to the ''Water/Vehicle'' group, and a cutoff of > 1.25 for transcripts whose translation were decreased in ''Alcohol/Rapamycin'' group compared to ''Alcohol/Vehicle'' group. P value was set at $p < 0.05$.

Quantitative real-time PCR

Total and polysomal RNA extracted from NAc were treated with DNase I. Synthesis of cDNA was performed using the AMV reverse transcriptase (Promega) according to the manufacturer's instructions. The resulting cDNA was used for quantitative real-time PCR. Thermal cycling was performed on an Applied Biosystem 7900HT Fast Real-Time PCR detection system (Applied Biosystems), using

a relative calibration curve. The quantity of each mRNA transcript was measured and expressed relative to *Glyceraldehyde-3-Phosphate deshydrogenase* (*GAPDH*). The following primers were designed using Primer3 software: *Prosapip1*: upstream 5′-GTC TGT CAG AAG GAG CAG GC-3′, downstream 5′-CCC CAC GAT CTC ACT CAA CT-3′; *Gucy1a3*: upstream 5′-CTT CCA CCA AAC TTC CCT A-3′, downstream 5′-GAA CCC ATT ACT TCA ACA CTT A-3′; *TAFA-3*: upstream 5′-AGA AGG TAA ATC AGC CAT AGT-3′, downstream 5′-ACA GAG GGT GAG CCA AGA-3′; *Tsnax*: upstream 5′-ATG TGC TCG CTC TAT TGT T-3′, downstream 5′-ATC GGT GAG AAA GGA AAA-3′; *GAPDH*: upstream 5′-CGA CTT CAA CAG CAA CTC CCA CTC TTC C-3′, downstream 5′-TGG GTG GTC CAG GGT TTC TTA CTC CTT-3′.

Western blot analysis

Cells and tissue were homogenized in ice-cold radio immunoprecipitation assay (RIPA) buffer (in mM: 50 Tris-HCl, 5 EDTA, 120 NaCl, and 1%NP-40, 0.1% deoxycholate, 0.5% SDS, proteases and phosphatases inhibitors). Samples were homogenized using a sonic dismembrator. Protein content was determined using BCA protein assay kit. Tissue homogenates were separated by 10% SDS-PAGE and transferred onto nitrocellulose membrane at 300 mA for 2 hours. Membranes were incubated with a blocking solution (5% milk-PBS, 0.1% Tween 20) at room temperature for 30 min and then probed with primary antibodies (anti-Prosapip1 antibodies 1/1000, anti-GAPDH antibodies 1/2000, anti-SPAR antibodies 1/1000, anti-actin antibodies 1/5000, anti-GFP antibodies 1/2000, anti-pS6K antibodies 1/1000, anti-S6K antibodies 1/1000, anti-p4E-BP antibodies 1/1000, anti-4E-BP antibodies 1/1000, anti-Flag antibodies 1/2000) diluted in blocking solution overnight at 4°C. Membranes were washed and probed with HRP-conjugated secondary antibodies for one hour at room temperature. Membrane were developed using ECL and band intensities were quantified using ImageJ software (NIH).

Crude synaptosomal fraction

Crude synaptosomal fractionation was conducted as described previously (Wang et al., 2010). Briefly, immediately after being collected, tissue was homogenized in a glass homogenizer containing 300 μL of ice-cold Krebs-sucrose buffer (in mM: 125 NaCl, 1.2 KCl, 1.2 MgSO4, 1.2 CaCl2, 22 Na2CO3, 1.2 NaH2PO4, 10 glucose, and 320 sucrose, as well as protease and phosphatase inhibitors, pH 7.4). The homogenate was centrifuged at 1.000 g for 10 min at 4°C to pellet heavy membranes and debris (P1). The supernatant (S1) was collected and was centrifuged at 16.000 g at 4°C for 20 min to pellet the crude synaptosomal membrane fraction (P2). P2 was re-suspended in 100 μL RIPA buffer. Protein concentration was determined using BCA protein assay kit.

Immunoprecipitation

Neuro2A cells and NAc punches were lysed in RIPA buffer and homogenized by centrifugation (10,000 g) for 10 min at 4°C. Immunoprecipitation was carried out by incubating the supernatants with anti-SPAR antibodies (1/250), anti-HA antibodies (1/250), anti-Prosapip1 antibodies (1/250) or anti-IgG control (1/250) overnight at 4°C followed by 1 hour incubation with protein A/G plus-agarose beads. Beads were washed out 6 times with the RIPA buffer. Protein samples were then subjected to SDS-PAGE and western blot analysis.

F-actin/G-actin assay

Actin reorganization assay was performed using the G-actin/F-actin assay kit (Cytoskeleton, Denver, CO), as previously described in (Huang et al., 2013) with small modifications. Neuro2A cells or NAc punches were homogenized in 250 μL cold LAS02 buffer with protease and phosphatases inhibitors, and centrifuged at 350 g for 5 min at 4°C to remove cellular debris. Protein concentrations were determined using BCA protein assay kit, and equal amounts of protein in supernatants were then centrifuged at 15,000 g for 30 min at 4°C to generate a new supernatant that contained soluble actin (G-actin). The insoluble actin (F-actin) in the pellet was re-suspended in 250 μL F-actin depolymerization buffer and incubated on ice for 1 hour, with gently mixing every 15 min. Samples were centrifuged at 15,000 g for 30 min at 4°C and the supernatant was used to measure F-actin. Twenty μL of the G-actin fraction and 40 μL of the F-actin fractions were loaded on an SDS-PAGE gel and analyzed by western blot analysis.

Plasmid constructs and preparation

HA-SPAR was a gift from Dr. D. Pak, Georgetown University, Washington, DC. Flag-Prosapip1 was cloned by high fidelity PCR using XhoI-Flag-Prosapip1 forward primer and XbaI-reverse primer and inserted into a modified form of the plvx-IRES-Zsgreen vector (Clontech, Cat. 632187) were Zsgreen has been replaced by GFP to obtain plvx-Flag-Prosapip1-IRES-GFP. To target Prosapip1 by shRNA, the 19 nucleotides short hairpin RNA (shRNA) sequence 5′-GGG AAG AGC TGG AGG ACA A-3′ targeting Prosapip1 (shProsapip1) was selected using siRNA Wizard v3.1 (InvivoGen, San Diego, CA). The scramble 19 nucleotides sequence 5′-GCG CTT AGC TGT AGG ATT C-3′ was used as a control (SCR). Synthesized DNA oligos containing the above sequences were annealed and inserted into pLL3.7 vector (Addgene, Cambridge, MA) at HpaI and XhoI sites. Plasmids DNA were prepared using a Plasmid Maxi Kit (Qiagen, Germantown, MD). All constructs were verified by sequencing.

Generation of lentivirus

The production of lentivirus was conducted as described in (Lasek et al., 2007). Briefly, HEK lentiX cells (Clontech, Mountain View, CA) were transfected with the lentiviral packaging vectors psPAX2 and pMD2.G, together with the pLL3.7 shProsapip1 or pLL3.7

SCR using lipofectamine 2000 (Invitrogen, Carlsbad, CA) in Opti-MEM medium (Sigma Aldrich, St. Louis, MO). Six hours after transfection, medium was replaced to DMEM-FBS 10%. Sixty hours after transfection, supernatant containing the viral particles was collected, filtered into 0.22 μm filters and purified by ultracentrifugation at 26.000 g for 90 min at 4°C. The pellet fraction containing the virus was resuspended in sterile PBS, aliquoted and stored at −80°C until use. Virus titer was determined using the HIV-1 p24 antigen ELISA kit (Zeptometrix, Buffalo, NY).

Intra-NAc Lentivirus infusion

Intra-NAc infusion of lentivirus was conducted as described in (Ben Hamida et al., 2012). Mice were anesthetized using isoflurane. Bilateral microinfusions were made using stainless steel injectors (33 gauge, Hamilton) into the NAc (anteroposterior +2.1 mm, mediolateral ± 0.75 mm and dorsoventral 4.30 mm, from bregma). Animals were infused with Ltv-SCR or Ltv-shProsapip1 ($1x10^8$ pg/mL (or $1x10^5$ pg/mL for dendritic spines analysis),1 μL/side) at an infusion rate of 0.2 μL/minute. After each infusion, the injectors were left in place for an additional 10 min to allow the virus to diffuse.

Immunohistochemistry

Immunohistochemistry was conducted as described previously (Ben Hamida et al., 2012). Specifically, mice were euthanized by CO_2 and transcardially perfused with 0.01M PBS followed by 4% paraformaldehyde (PFA) in phosphate buffer, pH 7.4. Brains were removed, fixed in 4% PFA overnight at 4°C, and then cryopreserved in 30% sucrose for 3 days. Brains were then rapidly frozen and coronally sectioned into 50 μm sections using a Leica CM3050 cryostat (Leica Biosystems). Sections were collected, washed in PBS and incubated at room temperature for 4 hours in PBS containing 5% normal donkey serum and 0.3% Triton X-100 for blocking and permeabilization, respectively. Sections were incubated in the primary antibodies at 4°C overnight (anti-NeuN 1/500, anti-GFP 1/500). Following washes, sections were incubated in secondary antibodies (donkey anti-chicken AlexaFluor 488 and donkey anti-mouse IgG AlexaFluor 564 antibodies,1/800) for 4 hours at 4°C. Sections were washed and then mounted onto Fisher Superfrost glass slides, ProLong Gold antifade reagent was added and slides were coverslipped. Images were acquired on a Yokagawa CSU22 Spining disk confocal microscope and NIS-Element Imaging software.

Morphological analysis

Mice underwent the IA20%-2BC paradigm for 4 weeks. Afterward, mice were divided in two groups with similar alcohol drinking consumption (16.3 ± 1.44 g/kg/24 hr and 15.3 ± 1.47 g/kg/24 hr) and Ltv-SCR or Ltv-shProsapip1 ($1x10^5$ pg/mL) was infused into the NAc (Figure 4A). One week after surgery, mice underwent 3 additional weeks of IA20%-2BC (7 weeks total). Alcohol intake values on the last week of drinking were 15.1 ± 1.57 g/kg/24h (Ltv-SCR) and 14.5 ± 0.97 g/kg/24 hr (Ltv-Prosapip1). Four hours after the beginning of the last drinking session (Figure 4A), mice were euthanized, perfused, processed, and 100 μm coronal sections were collected. Images of overall dendritic branches and the soma of GFP stained NAc shell neurons were acquired with a 20x objective with a z interval of 3 μm (30-35 images per cell). Images were reconstructed in 2D and GFP neurons were traced using Neurolucida software (MBF Biosciences, Williston, VT). Dendritic branches were quantified using Sholl analysis (Sholl, 1953), with the center of all concentric spheres defined as the center of the soma. Starting radius was 10 μm and end radius was 150 μm from the center of the soma with an interval of 10 μm between radii. For dendritic spines analysis, images were acquired with a 100x oil immersion lens. Individual neurons were chosen for spine analysis based on the following criteria: (i) There was minimal or no overlap with other labeled cells (ii) At least three primary dendrites needed to be visible for the cell to be used for analysis. (iii) Only distal dendrites (3^{rd} or 4^{th} order) of at least 25 μm long in focus plane were analyzed (Lee et al., 2006). Image z stacks of between 15 and 20 images were acquired at a z separation of 0.3 μm. Images of spines were deconvoluted by AutoQuant X3 (Media Cybernetics) (Wang et al., 2015), and morphological properties were analyzed by using FIJI software (NIH) (Smith et al., 2009). Protrusions from dendrites were classified into 4 types based on their length and neck and head morphology (Hering and Sheng, 2001). Filopodia were defined as long filamentous protrusions > 2 μm in length that lacked a discernable head. Stubby protuberances were defined as protrusions < 1 μm in length, with a head width > 0.3 μm that did not appear to have a neck. Mushroom-shaped spines were defined as dendritic protrusions < 2 μm in length, and characterized by a short neck and large spine head (head width > 0.5 μm). Thin spines were defined as protrusions < 2 μm in length that had elongated spine necks with small heads (head width < 0.5 μm). For each of the animals examined in each group, at least 7 neurons were analyzed, with at least 2 dendrites analyzed per neuron (Wang et al., 2015). The analysis was performed single-blinded by two experimenters.

Two-bottle choice drinking paradigm

Intermittent access to 20% alcohol

The intermittent-access to 20% alcohol two-bottle choice drinking procedure (IA20%-2BC) was conducted as previously described (Warnault et al., 2013) (Figure 1A). Briefly, mice were given 24 hours of concurrent access to one bottle of 20% alcohol (v/v) in tap water and one bottle of water. Control mice had access to water only. Drinking sessions started at 12:00 on Monday, Wednesday and Friday, with 24- or 48 hours (weekend) of alcohol-deprivation periods in which mice consumed only water. The placement (left or right) of water or alcohol solution was alternated between each session to control for side preference. Water and alcohol bottles were weighed at the beginning and at the end of each alcohol drinking session. Mice were weighed once a week. Seventy-80% of

the animals drank more than 14 g/kg/24 hr, and 6.5 ± 0.4g/kg/4 hr, a value that corresponds with blood alcohol concentration (BAC) of above 100 mg% (Hwa et al., 2011; Neasta et al., 2010), and were included in the study.

Continuous access to 10% alcohol

Mice had continuous access to two bottles (CA10%-2BC), one bottle containing a 10% alcohol solution (v/v) and the other containing tap water for 3 weeks (21 drinking sessions). The bottles were weighted every day at 12:00. Mice were weighed once a week. Mice consumed on average 7.4 ± 0.84 g/kg/24 hr and were considered moderate alcohol drinkers. All animals were included in the study.

Intermittent access to 0.01% saccharin

Mice underwent an IA-2BC paradigm as described above but had access to one bottle containing 0.01% saccharin solution in water and another bottle containing water only. Mice consuming water only were used as controls. Mice consumed on average 29.1 ± 9.9mL/kg/24 hr. All animals were included in the study.

Intermittent access to 1% sucrose

Mice underwent IA-2BC to 1% sucrose solution or water. Due to its palatability, sucrose 2BC results in an increase in the total amount of fluid intake during a 24-hours period (Gentry and Dole, 1987). To control for total fluid volume consumed, sucrose availability was restricted to 5 mL, which is equivalent to the total fluid intake observed during a 24-hour alcohol 2BC session. Mice consuming water only were used as controls. All animals were included in the study.

Chronic Intermittent Exposure to alcohol vapor

Mice underwent a chronic intermittent alcohol exposure (CIE) to alcohol in which alcohol was administered in vapor inhalation chambers as detailed previously (Becker and Lopez, 2004; Griffin et al., 2009). During a CIE cycle, mice were exposed to alcohol 16 hr/day for 4 consecutive days, which was followed by a 72-hr withdrawal period (Figure S5A). Mice underwent 2 CIE cycles. Before each of the 16-hours alcohol exposure, intoxication was initiated by the administration of alcohol (1.6 g/kg) combined with the alcohol dehydrogenase inhibitor pyrazole (1 mmole/kg in saline) i.p. in a volume of 0.02 mL/g body weight. The co-administration of pyrazole with alcohol is critical to maintain a high and stable level of intoxication during each cycle of alcohol vapor exposure (Griffin et al., 2009). An average BAC value of 175.5+/−10.6 mg % was obtained at the end of the second week of CIE exposure. Control mice were handled similarly, and were administered the same pyrazole dose prior to being placed in air inhalation chambers.

Electrophysiology recording

Sagittal slices (240 μm) were prepared in cutting solution containing (in mM): 225 sucrose, 119 NaCl, 2.5 KCl, 0.1 $CaCl_2$, 4.9 $MgCl_2$, 26.2 $NaHCO_3$, 1 NaH_2PO_4, 1.25 glucose, and 3 kynurenic acid). Slices were incubated at 33°C for 30 min and at room temperature afterward. Artificial cerebrospinal fluid (ACSF) containing (in mM): 124 NaCl, 2.5 KCl, 2.5 $CaCl_2$, 1.3 $MgCl_2$, 26.2 $NaHCO_3$, 1 NaH_2PO_4, and 20 glucose. Gabazine (5 μM) and d-serine (10 μM) were added to block GABAA-mediated responses and stabilize NMDAR-mediated responses, respectively. Whole-cell voltage-clamp recordings were obtained from fluorescently positive MSNs in the NAc shell using electrodes (2.5-3.5 MΩ) filled with solution (in mM): 130 $CsMeSO_4$, 10 CsCl, 10 HEPES, 0.2 EGTA, 4 Na-ATP, and 0.4 Na-GTP (pH = 7.25, ~290 mOsm). EPSCs were elicited by current pulses (0.2 ms width, every 10 s) using an ACSF-filled glass pipette placed 179.6 ± 7.0 μm (mean ± SEM, n = 32 cells) rostro-dorsally. Reversal potential for EPSCs was determined experimentally for each cell recorded and the holding membrane potential was set to +40 mV and −70 mV from the resting. The AMPA/NMDA ratio was calculated as the ratio of AMPAR-mediated EPSC amplitude at −70 mV to NMDAR-mediated EPSC amplitude at +40 mV. Spermine (0.1 mM) was included in the internal solution for measuring rectification index which was calculated as the ratio of AMPAR-mediated EPSCs at −70 mV to +40 mV which was then multiplied by 4/7 to normalize the two different driving potentials. Data were recorded with Multiclamp 700B (Molecular Devices), filtered at 1 kHz and digitized at 5 kHz. AMPAR-mediated EPSCs at +40 mV were recorded in the presence of the NMDAR antagonist, *(R)*-CPP (5 μM). NMDAR-mediated EPSCs were calculated by subtraction offline. mEPSC were recorded for 5 min in the presence of TTX (0.5 μM) and when holding the cell at −70 mV. Mini Analysis Program (Synapsoft) was used to automatically detect events with amplitude threshold of 5 pA. The ratios of area to amplitude of each detected events were calculated and the events with the ratio smaller than 2 or greater than 6 were eliminated.

Alcohol operant self-administration

Mice underwent IA20%-2BC for 7-8 weeks as described above. Mice that drank more than 14 g/kg/24 hr in the last week of IA-2BC were selected for the alcohol self-administration training. Prior to the beginning of the training, each animal was handled for 1 min per day for three consecutive days. Self-administration training was conducted during the dark phase of the reversed dark/light cycle in operant chambers (length: 22 cm, width: 20 cm, height: 14 cm) equipped with two levers (1.5 cm in length, 11 cm apart, 2.5 cm from the grid floor) mounted at the opposite ends of the same wall (Med-Associates; Georgia, VT). The operant chambers included a reward port centered between the levers (0.5 cm from the grid floor) with photo-beams to allow monitoring of reward magazine visits, a light centered above the reward magazine and a tone-delivering tweeter situated on the opposite wall of the levers. Each chamber was housed within a sound-attenuating box with a fan providing background noise and ventilation. Each chamber was connected to a computer to control and record program events. Mice underwent 5 daily self-administration sessions a week (Mon-Fri). Sessions started with the presentation of the 2 levers: responding on the active lever resulted in the delivery of a 20% alcohol via a motorized dipper that held 10 μL of liquid in the magazine. Reward delivery was paired with a 3 s tone (2900Hz) and the illumination of the cue-light above the magazine. Alcohol solution was delivered after 3 port entries have been made ensuring the consumption of

the previously delivered alcohol solution. The third reward port entry turned off the cue-light. Responding to the other lever, i.e., the inactive lever, had no programmed consequences. The number and timing of the active and inactive lever-presses, reward port visits and reward deliveries were recorded during each session (Figures S8A–S8C). Sessions ended with the retraction of the levers and the light was turned off. Self-administration training was initiated under a fixed ratio (FR) 1, i.e., one lever press results in the delivery of one reward, for three 6-hours sessions (10:00 – 16:00) followed by three 4-hours sessions (11:00 – 15:00). Afterward, the sessions lasted for 2 hours (13:00 – 15:00). Eight sessions under FR1 schedule followed by 8 FR2 sessions were conducted prior to surgery. Only mice that i) displayed a discrimination ratio between the active and inactive lever (number of active lever presses/ total active+inactive x 100) above 60%, which is an index of instrumental learning, and ii) self-administered more than 0.6 g/kg/2 hr, were included in the study. The high ratio (> 75%) of discrimination between the active and inactive lever reveals that the mice effectively learnt the operant task (Figure S8D). BAC measured at the end of the 2-hours self-administration session in a subset of mice showed a significant correlation between BAC and the amount of alcohol consumed (Figure S8E), indicating that mice reached pharmacologically relevant BAC when self-administering 20% alcohol.

Following stable responding under a FR2 schedule, mice were divided in 2 groups with similar number of active (91.6 ± 23.01 and 82.1 ± 9.15) and inactive (24.6 ± 8.01 and 17.7 ± 4.63) lever presses, port entries (125.8 ± 11.17 and 143.9 ± 15.13) and amount of self-administered alcohol (1.5 ± 0.18 and 1.5 ± 0.19 g/kg/2 hr) and were assigned to receive intra-NAc infusion of Ltv-shProsapip1 or the Ltv-SCR. Two weeks following surgery, alcohol self-administration was resumed for two additional weeks, allowing control mice infected with Ltv-SCR to reach a stable baseline of responding.

BAC measurements

At the end of a 2-hours operant alcohol self-administration session, mice were briefly anesthetized with isoflurane and blood was collected from the lateral tail vein with heparinized capillary tubes. Serum was extracted with 3.4% trichloroacetic acid and a 5 min centrifugation at 420 g. Alcohol content was assayed using the NAD-NADH enzyme spectrophotometric method using a Synergy HT spectrophotometer (Biotek, Hayward, CA) (Zapata et al., 2006). An Analox Instrument analyzer (Lunenburg, MA) was used to measure BAC at the end of a two weeks CIE vapor exposure and blood was sampled from the retro-orbital sinus. BACs were determined using a standard calibration curve.

Sucrose operant self-administration

Sucrose operant self-administration was performed in an independent cohort of mice. To avoid neophobia to sucrose, mice underwent 2BC access to 6% sucrose for 24 hours. Two days later, a 6-hour self-administration training session was initiated under a FR1 schedule using 6% sucrose as reinforcer.The duration of sessions and sucrose concentration were progressively decreased to 2 hours and 1%, respectively. Eight FR1 sessions followed by eight FR2 sessions were conducted prior to surgery (Figures S8G–S8I). Only mice that displayed a discrimination ratio between the active and inactive lever (number of active lever presses / total active + inactive x 100) above 60% were included in the study. Mice were pseudo-randomly assigned to receive intra-NAc infusion of Ltv-shProsapip1 or the Ltv-SCR contingent upon similar frequency of active (213.8 ± 33.33 and 205.4 ± 33.91) and inactive (47.5 ± 10.54 and 46.8 ± 11.17) lever presses, port entries (241.0 ± 31.49 and 237.9 ± 29.07) and 1% sucrose intake (21.9 ± 2.77 and 20.3 ± 2.80 mL/kg/2 hr). Two weeks following surgery, sucrose self-administration was resumed for two additional weeks.

Alcohol-induced Conditioned Place Preference paradigm

The conditioned place preference (CPP) procedure was conducted as previously described (Legastelois et al., 2015). The testing apparatus (Columbus Instrument) was housed in a dark sound-attenuating box and consists of a rectangular Plexiglas box (length 42cm, width 21cm and height 21cm) divided by a central partition into two equal chambers (21 × 21 × 21cm) equipped with horizontal photo beams. The compartments are distinguished by the walls color (black versus white) and the rough textured floor (stripped versus dotted). During the conditioning trials the individual compartments were closed off from each other. During the test sessions, the central partition was elevated from 4 cm above the floor of the apparatus, allowing the mice to enter both chambers. CPP testing was conducted during the light phase of the 12-hours light/dark cycle in a quiet room, dimly illuminated at 30 lux. Three weeks following intra-NAc infusion of Ltv-shProsapip1 or Ltv-SCR, each animal was handled for 1 min per day and habituated to an i.p. injection of a saline solution once a day for three consecutive days (Figure 7A). On the pre-conditioning day (day 1), mice were allowed to freely explore both chambers of the CPP apparatus for 30 min. Mice were then divided in 2 conditioning groups (saline or alcohol) with similar pre-conditioning time values in the preferred and the non-preferred compartment of the CPP apparatus. Conditioning training consisted of 8 daily conditioning sessions (days 2–9) during which mice were confined to one of the compartments for 5 min immediately following an i.p. injection of saline or alcohol (1.8 g/kg). On days 2, 4, 6, and 8 mice received a saline injection prior to confinement to the "unpaired" compartment. On days 3, 5, 7 and 9, mice received a systemic administration of saline (saline conditioning group) or alcohol (alcohol conditioning group), and were then confined to the "drug-paired" compartment. On day 10, mice were allowed to freely explore the CPP apparatus for 30 min (post-conditioning test) (Figure S7A). The time spent in each of the compartments was quantified by an automated system (Optomax, Columbus Instrument). The CPP score was calculated as the time spent in the drug-paired compartment during the post-conditioning minus the time spent in the same compartment during the pre-conditioning day.

Conditioned place aversion paradigm

The conditioned place aversion procedure was performed using the apparatus described in the CPP section and as previously described (Legastelois et al., 2015). Three weeks following intra-NAc infusion of Ltv-shProsapip1 or Ltv-SCR, each animal was handled for 1 min per day and habituated to a subcutaneous injection of a saline solution once a day for four consecutive days (Figure 7D). On the pre-conditioning day (day 1), mice were allowed to freely explore the entire apparatus for 20 min. Mice were then divided in 2 conditioning groups (saline or LiCl) with similar pre-conditioning time values in the preferred and the non-preferred chambers. Conditioning training consisted of 6 conditioning sessions with two conditionings per day (days 2–4) during which mice were confined to one of the compartments for 45 min immediately following an s.c. injection of saline or LiCl (130 mg/kg). On the morning of conditioning (starting at 8:00), mice received a saline injection prior to confinement to the ''unpaired'' chamber. During afternoon conditioning (starting at 15:00), mice received a systemic administration of saline (saline conditioning group) or LiCl (LiCl conditioning group), and were then confined to the ''drug-paired'' compartment. On the post-conditioning day (day 5), mice had free access to both compartments of the apparatus for 20 min (post-conditioning test). CPA score was calculated as the time spent in the drug-paired compartment during the post-conditioning minus the time spent in the same compartment during the pre-conditioning day.

QUANTIFICATION AND STATISTICAL ANALYSIS

Data were analyzed using the appropriate statistical test, including two-tailed unpaired t test, two-ways analysis of variance (ANOVA) or two-ways or three-ways repeated-measures ANOVA as detailed in the figure legends. Significant main effects and interactions of the ANOVAs were further investigated with the Student–Newman–Keuls post hoc test or method of contrast analysis. Data are expressed as mean ± SEM and statistical significance was set at $p < 0.05$. D'Agostino–Pearson normality test and *F*-test/Levene test were used to verify the normal distribution of variables and the homogeneity of variance, respectively. No statistical analysis was used to determine sample size *a priori*. The sample sizes chosen are similar to those used in previous publications (Barak et al., 2013; Neasta et al., 2010). The number of samples indicates biological replicates as indicated in each of the figure legends.

DATA AND SOFTWARE AVAILABILITY

Deposited data are available: http://dx.doi.org/10.17632/xzmp3zffz7.1.